Adaptive Distance Protection Scheme in Transmission Line with Renewable Plant

A THESIS

Submitted By

UJJAL BANIK
(*Roll No. M210469EE*)

In partial fulfilment for the award of the Degree of

MASTER OF TECHNOLOGY
IN
ELECTRICAL ENGINEERING
(POWER SYSTEMS)

Under the guidance of

Dr. Deepak M

DEPARTMENT OF ELECTRICAL ENGINEERING
NATIONAL INSTITUTE OF TECHNOLOGY CALICUT
NIT CAMPUS P.O., CALICUT - 673601, INDIA

JULY 2023

ACKNOWLEDGEMENT

I wish to express my gratitude to my project guide Dr. Deepak M, Assistant Professor, Department of Electrical Engineering, National Institute of Technology for the valuable guidance as well as timely advice which helped me a lot in doing the project and the Professor & Head of the Department of Electrical Engineering, Dr. Preetha P for providing the opportunities and facilities to work with. I would also like to extend my gratitude to Mr. Athul Jose P, Research Scholar, for the valuable guidance as well advice which helped me a lot in doing the project.

I would like to express my sincere gratitude to other panel members of M. Tech Project Power Systems, for their valuable guidance during the work. I take this opportunity to extend my sincere thanks to all the faculty members of the Department of Electrical Engineering for sharing their valuable comments during the preparation of the project.

UJJAL BANIK

DECLARATION

I hereby declare that this submission is my own work and that, to the best of my knowledge and belief, it contains no material previously published or written by another person nor material which has been accepted for the award of any other degree or diploma of the university or other institute of higher learning, except where due acknowledgment has been made by me in the text.

Place: Kozhikode
Date: 04/07/2023

Name: UJJAL BANIK
Roll No: M210469EE

CERTIFICATE

This is to certify that the thesis entitled "**Distance Protection in Transmission Line with Renewable Plant**" submitted by **Mr. UJJAL BANIK (Roll No.M210469EE)** to the National Institute of Technology Calicut towards partial fulfilment of the requirements for the award of **Degree of Master of Technology in Electrical Engineering (Power Systems)** is a bona fide record of the work carried out by him, under my/our supervision and guidance.

Dr Deepak M
(Guide)
Asst. Professor
Dept. of Electrical Engineering

Attested by

Dr Preetha P
Professor & Head
Dept. of Electrical Engineering

Place: Kozhikode
Date: 04/07/2023

ABSTRACT

Photovoltaic (PV) plants operate in DC. Therefore, to connect large PV plants with an AC grid, a converter is inserted in-between the grid and the renewable source. Converter does all the necessary modification and matching, so that PV plant can be incorporated with conventional grid. Various grid codes (GC), like European Union grid code, North American grid code are employed in renewable plants. Control mechanisms (Current limit control, Low voltage ride through control etc) are present to meet the grid code standards. When converters are modified with those control strategies, it creates challenges in distance protection as it is solely dependent on the voltage and current data. Relay fails to detect the fault as apparent impedance (impedance seen by the relay) variation is very less during fault. Challenges brought by the control schemes have been analysed and as a solution adaptive distance scheme is incorporated with conventional distance protection method. Functionality of adaptive scheme has been verified with mho relay in PSCAD/EMTDC.

Keywords: - Converter-interfaced renewable energy plants (CIREPs), distance protection, fault in transmission line, inverter control scheme.

CONTENTS

List of Abbreviations

CB	-	Circuit Breaker
CIREP	-	Converter Interfaced Renewable Energy Plant
EHV	-	Extra High Voltage
GC	-	Grid Code
LVRT	-	Low Voltage Ride Through
MPPT	-	Maximum Power Point Tracking
PSB	-	Power swing blocking
PV	-	Photo Voltaic
RES	-	Renewable Energy Source
SG	-	Synchronous Generator

List of Symbols

α	-	Dimension less quantity with unity magnitude and angle of 120^o
I_m	-	Current from the CIREP side
I_n	-	Current flowing from the grid side
R_g	-	Fault Impedance
ΔZ	-	Additional Impedance
Z_{app}	-	Impedance calculated by relay
Z_F	-	Line impedance up to fault point
θ_L	-	Angle associated with line impedance

List of Figures

CHAPTER 1
INTRODUCTION

1.1 Background

Generation of electrical power is one of the major causes of environmental pollution. More than 75% of the generation are coming from fossil fuel and nuclear plants. To generate nuclear energy, radioactive materials are used. It causes radioactive wastes and radiation. Transportation and disposal of such chemical is also difficult. For fossil fuel plants CO_2, SO_2, NO_X are common products. SO_2 is one of the reasons of acid rain. Different greenhouse gases production cause global warming. These two sources are leading cause of air water and land pollution.

As a solution of above-mentioned problems renewable energy comes as a saviour. Renewable energy can be extracted from natural resources. It can be used seamlessly (Like, sunlight and wind), without causing hazard for earthly resources (such as coal, oil, gas, radioactive chemicals). It results, very less amount of greenhouse gases emission.

Mega Watts rated solar and wind farms are being installed to supply energy. These renewable plants are being connected with grid to satisfy our energy need. As per the report on 2021, globally 849.5 GW of electricity is being generated from solar energy run plants. The number is 824.9 GW for wind plant.

In case of solar power plant, energy coming from solar irradiation is converted into electrical energy by using photovoltaic panels. Such solar panels are installed in large number parallelly and in series to form a large plant. The harvested thermal energy is converted into Direct Current (DC) electricity by means of PV panel. Alternating Current (AC) is used in grid. To convert this produced DC energy into AC, an extra component Inverter becomes essential here.

The primary intention of power system protection is to remove the faulty part out of the system to protect the remaining healthy part. There are different protection equipment; like, circuit breaker, isolator, lightning arrester, relay etc. If there is a fault, relay senses the fault and it instructs the CB to trip. As a result, flow of fault current can be prevented.

The relay is the brain of power system protection. If at a certain instant, the values of the actuating quantities (Voltage, Current, Impedance etc) associated with the relay, crosses the threshold value, the relay operates. There are different characteristics, logics are present for protection relay to operate. These logics are employed based on the situation and field. For unit protection Differential relays are suitable, for transmission line protection distance relays are preferred. The working principle of a distance relay is determined by the voltage that is measured by PT and the current measured by CT. It calculates the impedance and operates based on the logic within it. There are various kinds of distance relays present, such as mho relay, impedance relay, reactance relay etc.

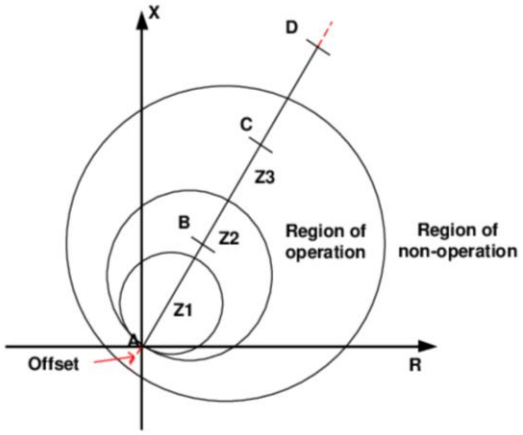

Fig: 1.1 Mho circle in R-X plane with different Zones

Mho relay is voltage-controlled admittance relay. These are generally used in EHV, long transmission lines protection. It gives direction protection as an extra feature. These are more sensitive as it measures both distance and direction. If the impedance measured by the relay is less than the set value for the respective relay, it means there is a fault in the system. The diameter of each circle is the impedance setting for each relay. In power system different transmission lines are present. The primary mho relay protects only 85% of the line (First circle, No time delay). Second, third circle is for back up protection. They are differentiated with proper time delay. If the measured impedance falls within the circle, the relay trips.

1.2 Motivation:

Photovoltaic plants generate power in DC. Most of the grids are running in AC. To connect large PV plants with the grid, a converter in-between the grid and the renewable source is used. Fig 1.2 is a single-line diagram for CIREP connected with a grid. All the PV source units are connected to a power electronic converter. The output voltage of those converters is modified with transformer action, according to the transmission line demand. This converter does all the necessary modification and matching, that a PV plant can be incorporated with a conventional grid. These renewables are depending on natural resources which are uncertain and variable. As a result, power fluctuation can be observed. MPPT technologies are used to extract the maximum possible power out of the plant for the given natural resources at the current instant. There are different grid codes, like the European Union grid code, North American grid code, etc. In power plants, various control mechanisms are employed to meet the grid code standards. Like, Current limit control, Low voltage ride-through control, etc.

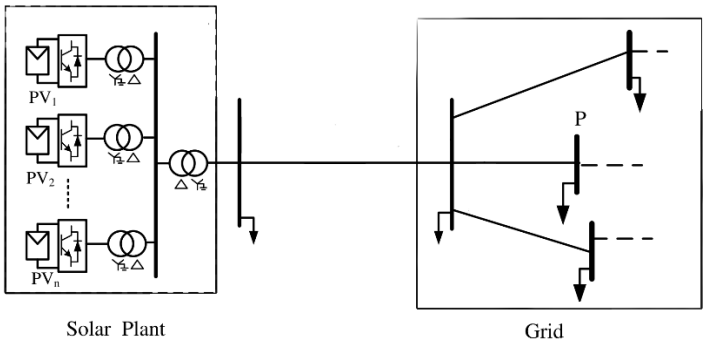

Fig 1.2: Typical single line diagram of CIREP with grid

A. Current Limit Control

Transient condition present in grid may affect the power electronic components present inside an inverter. Short circuit faults are common scenario for a power system every day. Such nuisance badly affects the functionality of the inverters. To protect them, some control and operational remedies are provided. To protect this power electronics devices from the over current condition, the output current passing from the inverter is controlled to be within a limit.

B. Low voltage ride through control

Renewable generators used to be removed from the grid in the event of a grid voltage dip in the past. However, now a days such renewable plants are holding a large amount of share in overall

power generation. Disconnection of renewable plant in such condition may lead blackouts. To stand against the situation, LVRT control is taken. Here, CIREPs are not disconnected in case of voltage dip and they stay within the system.

Such control strategies modulate the current and voltage at the CIREPs output. It causes maloperation of distance relay, which is connected in the transmission lines coming out of CIREPs.

1.3 Literature Survey

Recent situation has led the world to go for megawatts of renewable energy plants which are connected with grid by means of converter interface. To ensure the safety of converters present in CIREPs, different control strategies are employed. As a result, modern grid codes (GC) are stressing to employ LVRT capabilities [1]. Besides LVRT capability, modern GCs are also ensuring that CIREPs are adhere to meet active and reactive power. Not only the power generation at normal operation but also give reactive power support at faulty condition [2]. Because of the influence of control strategies, the fault characteristics differs from the conventional synchronous generator present in grid. Analysing the short circuit current from the CIREPs, the grid-side boosting current has a significant impact on the measured impedance at CIREP side, which results in a large amplitude and phase offset. [3]. As a result, there is a significant discrepancy in the impedance computed by the relay (Zapp) from line impedance up to the fault location (ZF). Due to this the impedance moves towards the negative imaginary axis and it may settle in the fourth quadrant of the RX plane. As a result, the fault cannot be located in the appropriate zone of the relay setup. The proper operation of traditional distance protection may be hampered by differences between the fault behaviours of synchronous sources and PV power plants. PV power plants' positive- and negative-sequence fault current amplitudes are substantially less than those of synchronous sources. Distance relays are prone to underreach or overreach issues because of the presence of fault resistance, which results in inaccurate distance relay operation. [4]. When fault resistance is present in the fault loop, distance relays may malfunction or fail to operate at all, which poses a serious risk to the power system's safety. To cope up with the situation different techniques has been suggested in literatures. Scheme based on time delay and zero-sequence impedance may be employed [3]. Without communicating with the other side, the mentioned system can precisely identify the fault. It has excellent adaptability to fault resistance with acceptable speed and selectivity and can discriminate between internal and

external faults. There is a significant possibility that a distance relay with a standard mho or quadrilateral characteristic will mistakenly identify both internal and external faults. The general expression of adaptive setting impedance is determined by using the geometric relationships in between measured impedance, added impedance, setting impedance, and adaptive setting impedance [4]. High-frequency fault component-based distance protection can also be employed as a efficient solution [5]. CIREPs show fault characteristics like the weak infeed, current frequency offset, and unstable internal impedance, therefore the distance protection on the RES side has a high risk of refusal. To address the issue of unstable internal impedance of CIREPs, the high-frequency impedance model of CIREPs has been developed. On this basis, the high-frequency operating voltage and the high-frequency voltage at the fault spot can be accurately compared to identify internal and external faults. The suggested method may run at a high speed and is mostly unaffected by control schemes. With each new sample of voltage and current data feeding to the relay, the method described in [6] determines the phase angle of the faulted loop current by determining the pure-fault sequence impedances of the renewable plant.

Due to the Grid-side voltage source converter's fast reactive power control, the backup distance protection relay is prone to overestimating the fault distance when a three-phase fault occurs in a transmission line close to the PCC bus of an HVDC system. To address relay overestimation in the HVDC-connected ac grid, the second zone of distance relays were previously readjusted. A robust controller for the HVDC system has been proposed in [7].

Mutual coupling effect has an impact on the effectiveness of parallel transmission lines' protection. One of the main problems for protection, which could lead to the malfunction of conventional distance relays, is the mutual coupling of nearby transmission lines. In order to protect mutually connected transmission lines, [8] presents an adaptive zero sequence compensation technique.

A distant relay's operational weakness is seen in the third zone. Due to issues like load encroachment and infeed current, the third zone may under-reach and not function as planned. In order to eliminate the zone under-reach caused by the infeed currents, a technique for adaptive expansion of a distance relay's third zone is suggested in [9]. Synchronized measurements of voltages and currents taken at the relay's location and at the endpoints of all nearby lines allows the 3rd zone to be extended properly and the infeed currents to be identified. The calculated extension covered the full length of the adjacent lines in all of the cases.

1.4 Problem Formulation

It is clearly visible, what are the problem may occur in protection scheme, if CIREPs are there in a grid. The problem can be further analysed to visualize in lucid manner.

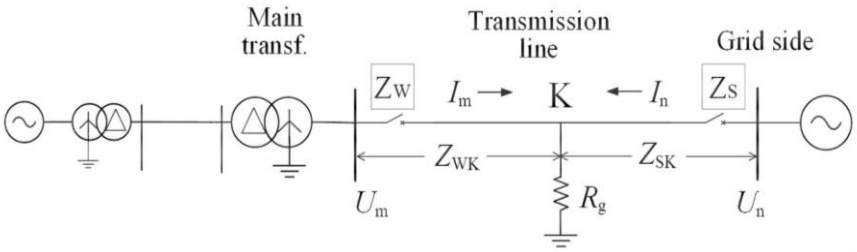

Fig: 1.3 Two bus system with CIREP

As per the given Fig 1.3, I_m is the current from the CIREP side and I_n is the current flowing from the grid side. A fault has occurred at K position with fault impedance of R_g. The distance relay present at the CIREP side sees impedance Z_W and at grid side it is Z_S. While, there is a fault at K, the impedance seen by the CIREP side distance relay is,

$$Z_W = \frac{U_m}{I_m} = \frac{I_m Z_{WK} + (I_m + I_n) R_g}{I_m} = Z_{WK} + (1 + \frac{I_n}{I_m}) R_g \quad (1.1)$$

$\left(1 + \frac{I_n}{I_m}\right) R_g = \Delta Z$, this quantity indicates the additional impedance. Equation (1.11) is simplified as,

$$Z_W = Z_{WK} + \Delta Z \quad (1.2)$$

During fault, I_m is 1.5-2 times the full load current but I_n is about 10 times the normal current. As a result, the factor ΔZ becomes very high. This results in a large difference between Line impedance up to fault point from bus and Apparent impedance calculated by relay.

Theoretically, the phase angle of (I_n/I_m) may vary from 0° to 360°, due to the time-varying current of CIREPs [3]. The ΔZ will be expressed as a large inductive one, if the range is between 0° and 180°. As a result, in case of internal faults, the grid-side distance relay will mal operate. The ΔZ will be expressed as a large capacitive one, if the phase angle is between 180° and 360°, results the CIREP-side distance relays to maloperate.

1.5 Objectives

The main objectives of the thesis are as follows:

- Identify the challenges in distance protection scheme while CIREPs are connected with conventional grid.
- Look into inverter control strategies to address the situation in CIREPs
- Study, how the impedance measured by the relays during the fault varies when CIREPs are delt within the system.
- Propose an optimal method/algorithm that would mitigate the possible hazards raised by the CIREPs and calculate the actual impedance irrespective of the control strategies employed with inverters.
- Verify obtained results with real-time hardware in loop system.

1.6 Outline of the Report

The report is structured as follows. Chapter 2 deals with the detailed discussion on distance protection scheme. Where calculation of different fault resistance and mho, quadrilateral relay characteristics are also elaborated. Adaptive distance protection scheme is discussed in chapter 3. Equations are derived for three phase fault. In Chapter 4, the obtained results are analysed and discussed. Chapter 5 covers the hardware implementation part, its background, and outcomes. Ultimately, a summary of the results and future scopes are presented in Chapter 6.

CHAPTER 2
Distance Protection of Power Systems

2.1 Introduction

Distance relays compare local current and local voltage to determine the impedance of the line that has to be protected. The distance relays may always be configured for instantaneous operation in the first zone because they achieve selectivity based on impedance rather than current. Setting up a distance relay is generally simpler. Distance relays are used for long, extra-high-voltage transmission lines that carry electricity at 132 kV, 220 kV, and 400 kV due to these advantages. Distance protection would not be financially feasible for 11 kV transmission lines and 66 kV distribution lines; thus, overcurrent relays are utilised instead. Overcurrent relays are used as backup protection relays for extra-high voltage lines. Different current and voltage configurations can produce various characteristics, including impedance, ohm, reactance, and mho. Distance relays basically evaluate local voltage (voltage at the relaying point) and local current to determine the impedance from the relaying point to the fault point. These relays are referred to as distance relays, since the impedance is related to the distance to the fault spot.

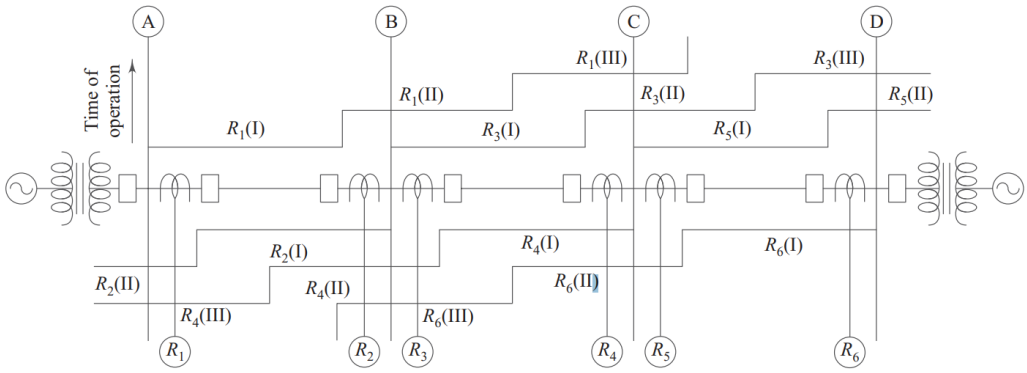

Fig 2.1 Stepped distance characteristics of distance relays

Stepped distance characteristics in advance relays enable back-up protection in distance protection. A distance relay provides three zones of protection in such a protection architecture, as depicted in Fig 2.1. The image makes it abundantly evident that each distance relay is built to be

configured for three separate zones. Approximately 80% of the area to be protected is covered by the first zone. If the fault is in the first zone, a distance relay operates right away. The first line section and roughly half of the next line section are included in the second zone. If the fault occurs in the second zone of protection of the relay, the same distance relay starts up after a certain amount of time. As shown in the Fig 2.1, if the protective relaying equipment is unable to instantly remove a defect at the relaying point R3, the relay R1 would operate in the second zone. Without a doubt, the second zone of the relay R1 does not cover the entire second line segment. However, since the third zone of the relay R1 covers the entire second-line segment, it does serve as a backup.

A distance relay should measure the positive sequence impedance of the transmission line, from the relaying location to the fault. This measurement must not change for a specific fault occurrence, regardless of the fault type (LLLG, LLG, LG, or LL fault).

There are ten different type of faults, that can occur on a three-phase power system; three phase faults, three phase-to-phase faults, three phase-to-ground faults, and three double-phase-to-ground faults. For each of these faults, a particular set of equations governs the relationship between the voltages and currents at the relay point. It is vital to distance relaying that the voltage and current used to power the proper relay are such that it will measure the positive-sequence impedance to the fault. Once this is accomplished, regardless of the fault type, all relay zone settings can then be based on the line's overall positive-sequence impedance.

2.2 Phase-to-Phase Faults

2.2.1 Apparent Impedance Calculation

A fault on a three-phase transmission line, that occurs between phases B and C. Fig 2.2 displays the symmetrical component representation for this fault. The positive- and negative-sequence voltages at the fault bus are equal, and expressed as,

$$E_{1f} = E_{2f} \tag{2.1}$$

$$E_{1f} = E_1 - Z_{1f}I_1 \tag{2.2}$$

$$E_{2f} = E_2 - Z_{1f}I_2 \tag{2.3}$$

where I_1, I_2, E_1, E_2 are the symmetrical components of currents and voltages at the relay location. The positive- and negative-sequence impedances of the transmission line are identical.

using the above equations,

$$\frac{E_1-E_2}{I_1-I_2} = Z_{1f} \tag{2.4}$$

since at the relay location the phase quantities are given by

$$E_b = E_0 + \alpha^2 E_1 + \alpha E_2 \text{ and } E_c = E_0 + \alpha E_1 + \alpha^2 E_2$$

Then,

$$(E_b - E_c) = (\alpha^2 - \alpha)(E_1 - E_2) \text{ and } (I_b - I_c) = (\alpha^2 - \alpha)(I_1 - I_2)$$

Therefore,

$$\frac{E_b-E_c}{I_b-I_c} = \frac{E_1-E_2}{I_1-I_2} = Z_{1f} \tag{2.5}$$

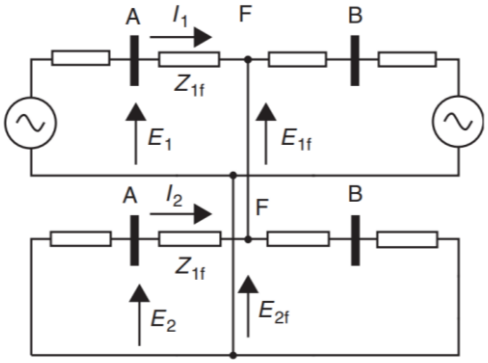

Fig: 2.2 Symmetrical component circuit for BC fault

2.3 Phase to Ground Faults

2.3.1 Apparent Impedance Calculation

The symmetrical component connection diagram is as depicted in Fig 2.3 for a fault between phase A and ground. In this instance, the voltages and currents at the relay site are,

$$E_{1f} = E_1 - Z_{1f}I_1 \tag{2.6}$$

$$E_{2f} = E_2 - Z_{1f}I_2 \tag{2.7}$$

$$E_{0f} = E_0 - Z_{0f}I_0 \tag{2.8}$$

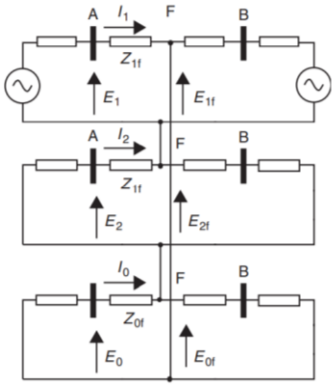

Fig: 2.3 Symmetrical component circuit for an AG fault

The symmetrical components can be used to express the phase a voltage and current, and the voltage of phase an at the fault location can be set to zero:

$$E_{af} = E_{0f} + E_{1f} + E_{2f}$$

$$E_{af} = (E_0 + E_1 + E_2) - Z_{1f}(I_1 + I_2) - Z_{0f}I_0 = 0$$

$$E_{af} = E_a - Z_{1f}I_a - (Z_{0f} - Z_{1f})I_0 = 0$$

where I_a is equal to ($I_0 + I_1 + I_2$) in Equation. Finally;

$$I_1' = I_a + \frac{Z_{0f} - Z_{1f}}{Z_{1f}} I_0$$

$$I_1' = I_a + \frac{Z_0 - Z_1}{Z_1} I_0$$

$$I_1' = I_a + mI_0 \qquad (2.9)$$

The whole line's zero and positive-sequence impedances are Z_0 and Z_1, respectively. A compensation factor, 'm' is used to account for the mutual coupling between the faulted phase and the remaining two unfaulty phases. It compensates the phase current.

For a phase-a-to-ground fault;

$$\frac{E_a}{I_a + mI_0} = Z_{1f} \qquad (2.10)$$

2.4 Three Phase Faults

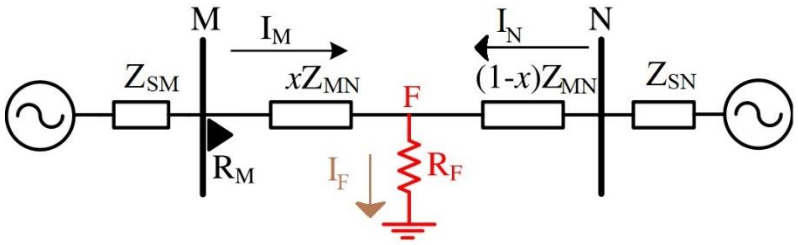

Fig: 2.4 Two bus system with fault at x distance from the relaying point

2.4.1 Apparent Impedance Calculation

For a three phase to ground fault, $E_{af} = E_{bf} = E_{cf} = 0$

Voltage seen by the relay present at M is,

$$E_{aM} = I_{aM}\, xZ_{1MN}$$

$$E_{aM} = I_{bM}\, xZ_{1MN}$$

$$E_{aM} = I_{cM}\, xZ_{1MN}.$$

xZ_{1MN}= Positive sequence impedance up to fault point.

$$xZ_{1MN} = \frac{V_{aM}}{I_{aM}} = \frac{V_{bM}}{I_{bM}} = \frac{V_{cM}}{I_{cM}} \quad (2.11)$$

$$Z_{app} = \frac{V_{aM}}{I_{aM}} \quad (2.12)$$

2.5 Distance Relay Implementation

The block diagram representation of the distance protection scheme is presented in Fig 2.5. Voltage and current are converted in measurable dimension using CT and PT at the very beginning. ADC is implemented to convert the analog data into digital according to the settings. Based on the value of the voltage and current fault detection happens. After the process, apparent impedance is calculated using the equation discussed in the section 2.2, 2.3 and 2.4. Once it is completed, the impedance value is checked, whether it lies in restrain or trip region. Based on the location, relay makes the decision. To discuss the process of relay operation the 2-bus system, Fig 2.4 is referred. The distance relay calculates the positive sequence impedance up to the fault point. The relay is set according the positive sequence impedance and the desired zone reach (for zone 1 it is up to 80%).

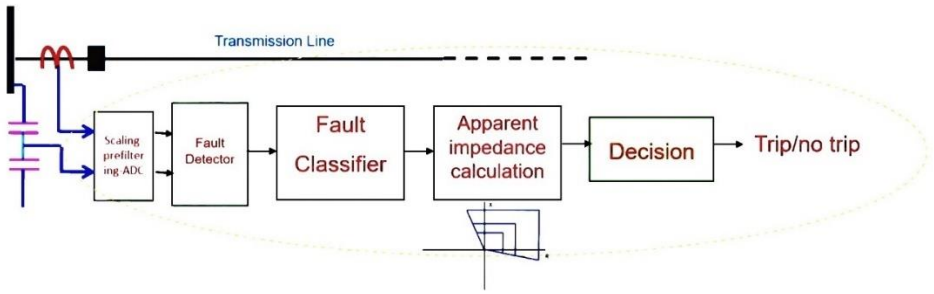

Fig 2.5 Distance Protection Scheme in One Line

Fig 2.6 shows the line MN and the impedance in R-X plane. If the system is loaded and the power factor near 1, then the operating point is expected to be situated far from the impedance line MN. If a fault happens in between the line MN, then the voltage will go down and the current will go up. Therefore, the impedance seen by the relay will be very less and if the fault resistance R_f is 0, then the possible point is displayed in Fig 2.6.

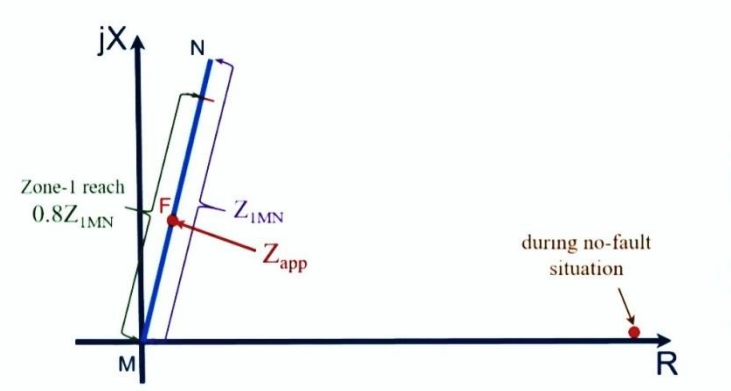

Fig 2.6 R-X plane with MN line impedance

In case of a fault, the fault resistance R_f comes in consideration. Taking this parameter in to account Fig 2.7 is given. When I_N flowing from the right-side source is neglected and the arc resistance during the fault R_f is considered the impedance seen by the relay i.e. Z_{app} is shown in Fig 2.7.

Therefore,

$$Z_{app1} = xZ_{1MN} + R_{f,}$$

where, $R_f \neq 0$ and $I_N = 0$

When the right-side source supplies the fault current is,

$$I_f = I_M + I_N.$$

At this scenario,

$$Z_{app2} = xZ_{1MN} + (I_f/I_M)\, R_f$$

where, $R_f \neq 0$ and $I_N \neq 0$

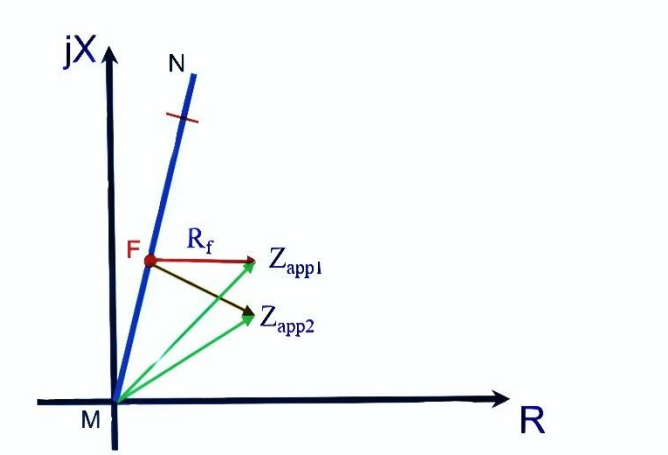

Fig 2.7 Apparent impedance with fault resistance in R-X plane

Generally, for numerical relaying operation in distance protection scheme mho and quadrilateral relays are useful.

2.6 Mho Relay Characteristics

As per the design, if at any instant the impedance comes inside the mho cycle, then the relay trips. The reach of the relay is set by the operator, according to the parameter of the line. Therefore, Z_R (zone 1 reach impedance) is user defined parameter. If a fault happens at the reach of the system and the impedance seen by the relay is Z_{app}, then $\Delta Z = Z_R - Z_{app}$. The position of Z_{app} is shown for faults happening inside and outside of the zone (Fig 2.8(a)). From Fig 2.8, it can be observed that, if the angle between Z_R & Z_{app} is equal to 90^o the is happening at the reach, the angle is less than 90^o the fault present inside the zone and when the angle is greater than 90^o the fault present outside the zone.

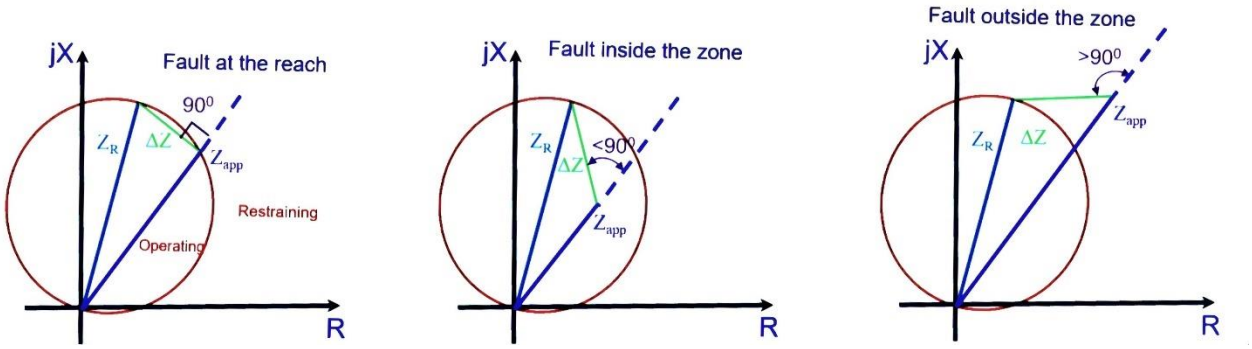

Fig 2.8(a) MHO circle and different impedance in RX plane

So, this concept is elaborated in Fig 2.8(b & c). From here it can be written that,

$$Operate:\ -90° < angle(\frac{\Delta Z}{Z_{app}}) < 90°$$

$$Restrain: 90° < angle(\frac{\Delta Z}{Z_{app}}) < -90$$

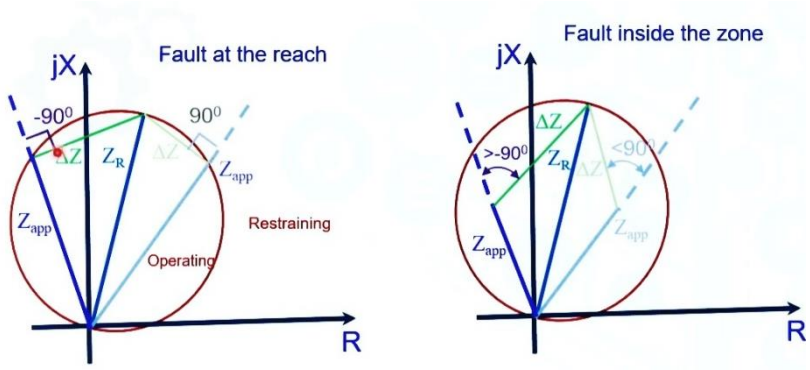

Fig 2.8(b) MHO circle and different impedance in R-X plane

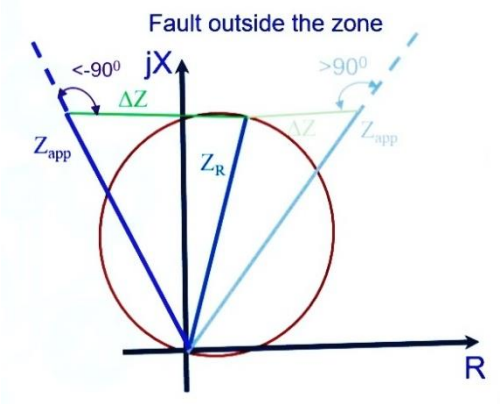

Fig 2.8(c) MHO circle and different impedance in R-X plane

Now multiplying all the impedances with I_M,

$$V_M = I_M Z_{app}$$

$$\Delta V = I_M \Delta Z.$$

Using above equations, δ is defined as δ = *angle* (ΔV) - *angle* (V_M).

Therefore, it concludes,

$$Operate: \ -90° < angle(\delta) < 90°$$

$$Restrain: 90° < angle(\delta) < -90°$$

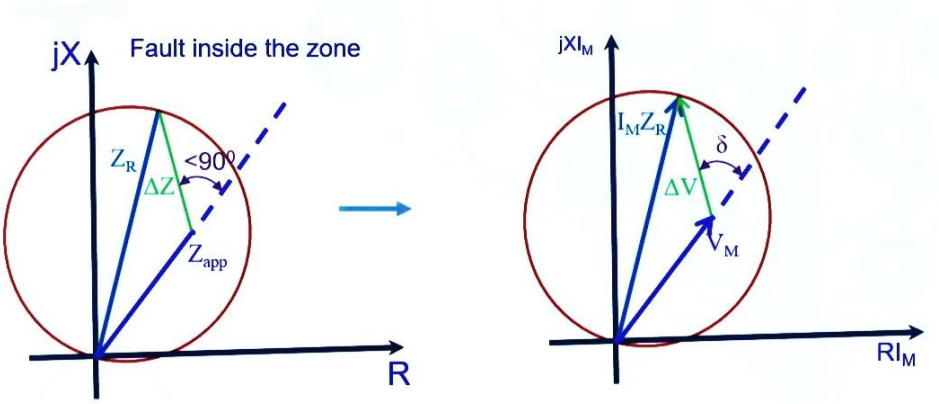

Fig 2.8(d) MHO circle and different impedance in R-X plane

2.7 Quadrilateral Relay Characteristics

In Fig 2.9, line 1 of the diagram corresponds to transmission line impedance Z_R. With line 2, fault at relay reach point with different fault resistance R_F is taken in account. Line 3 signifies fault at different location of the line with fault resistance of R_F. Line 4 is fault impedance at relay point with different fault resistance. The operating region lies inside the quadrilateral. Here, the width of the diagram can be designed depending upon the fault resistance. However, increasing the width to take care of the fault resistance may cause the quadrilateral to situate near the load point. Despite of the issue, there are few more factors need to be taken care of. Therefore, a modulated quadrilateral characteristic is shown in Fig 2.10.

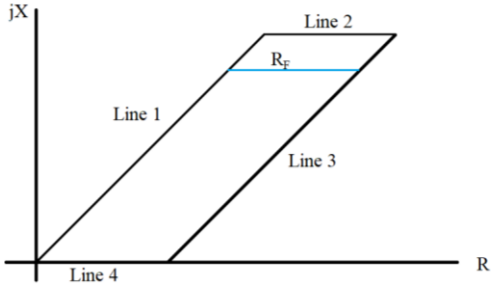

Fig 2.9 Simple Quadrilateral characteristics in R-X plane

It is seen that φ_1, φ_2, φ_3 these three angles have been introduced in the modified quadrilateral relay characteristics. φ_1 solves the problem of over reach, caused by the fault resistance R_F. Angle φ_2 takes care of the maloperation in loading condition. When the faults are near to the relay point, φ_3 ensures the reliable performance of the distance protection. The angle φ_3 increases the operation zone.

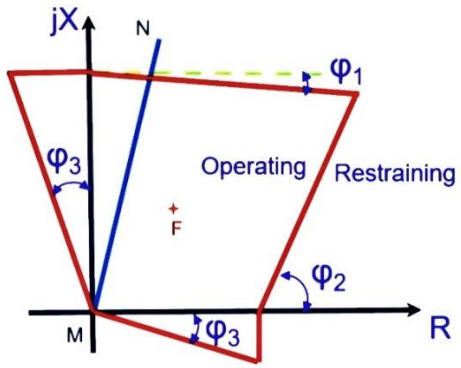

Fig 2.10 Modified quadrilateral characteristics in R-X plane

Typical values are φ_1=7°, φ_2=60°, φ_3=15°.

2.8 Summary

For transmission line protection distance relaying scheme is suitable. Mho and quadrilateral relays are two popular type of distance relays. Disadvantages identified with mho characteristics are neutralized by introducing quadrilateral relay, with modified operating area. Such modification is easy with numerical type relay. To detect the fault, the relay measures the apparent impedance at the relaying point. For different type of fault, there are different apparent impedance calculation methods depicted in section 2.2-2.4. Traditional relays face difficulties with CIREP, to mitigate adaptive distance protection is discussed in next chapter.

CHAPTER 3:

Adaptive Distance scheme

3.1 Introduction

Relays present at CIREP side, usually face difficulty in identifying the occurrence of a fault. The impedance calculated by the relay, remains outside of the protection zone, defined for the relay. Therefore, the working area for the relay has to be modified based on the condition of respective moment of a fault. To be more specific, the working area won't be constant what used to be used for conventional distance protection. Rather, the trip zone would be modified based on few equations, derived in this chapter. This new distance protection approach to identify fault is Adaptive Distance Scheme.

3.2 Description of Adaptive Scheme

A two-bus system has been discussed to establish all the equations needed to implement an adaptive algorithm in Fig. 3.1.

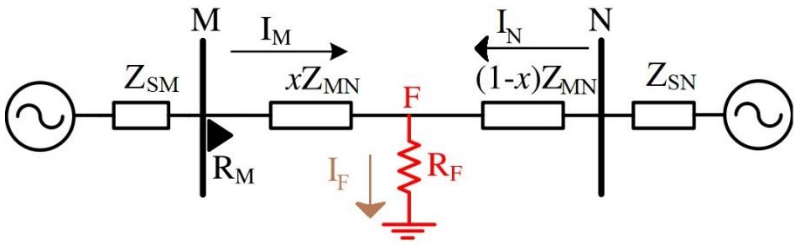

Fig: 3.1 Two bus system with fault at x distance from the relaying point

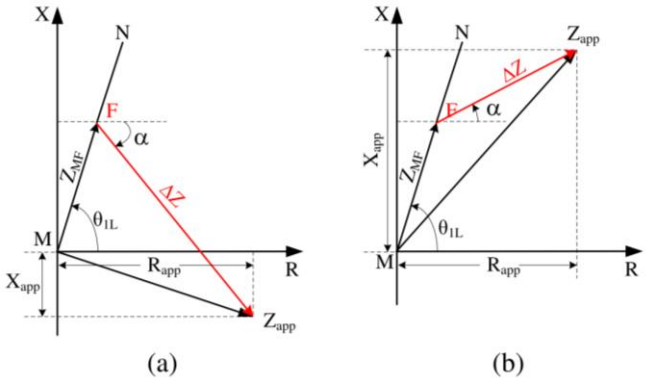

Fig. 3.2 Impedance diagram of distance relaying with CIREP (a)I_M leading and (b)I_M lagging to the current in the faulted loop.

Fig 3.2, the impedance diagram of distance relaying with CIREPs. θ_{1L} is the angle associated with the line impedance(Z_{1L}). Z_{app} is the impedance seen by the relay. Using geometry angle α can be obtained as,

$$\alpha = \tan^{-1}\left(\frac{|Z_{MF}|\sin\theta_{1L} - X_{app}}{|Z_{MF}|\cos\theta_{1L} - R_{app}}\right) \tag{3.1}$$

Z_{MF} is the impedance from relaying point M to the fault point F. Z_{MF} can be obtained as,

$$Z_{MF} = \frac{X_{app} - R_{app}\tan\alpha}{\sin\theta_{1L} - \cos\theta_{1L}\tan\alpha}(\cos\theta_{1L} + \mathrm{j}\sin\theta_{1L}) \tag{3.2}$$

If α is calculated correctly, Z_{MF} can easily be determined from equation 3.2. α is a function of fault current I_F. The adaptive algorithm calculates the α from the local data (data obtained from the relay bus).

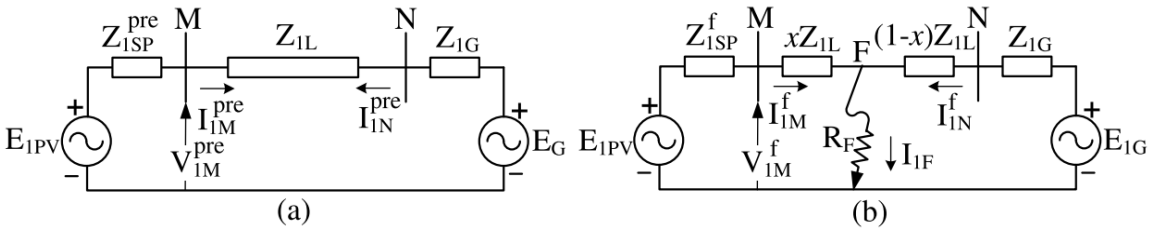

Fig: 3.3 Equivalent model of CIREP network at (a) pre-fault and (b) fault condition.

For the circuit in Fig. 3.3(b) using Kirchhoff's current law, the faulted loop current through R_F can be expressed as,

$$I_{1F} = I^f_{1M} + I^f_{1N} \tag{3.3}$$

The fault currents at bus M and N are I^f_{1M} and I^f_{1N} respectively.

Currents are equal in magnitude, however, opposite in phase at both ends during pre-fault, as shown in Fig. 3.3(a). Thus, equation no. (3.3) can be rewritten as

$$I_{1F} = \Delta I_{1M} + \Delta I_{1N} \tag{3.4}$$

Therefore,

$$\Delta I_{1M} = I^{f}_{1M} - I^{pre}_{1M} \quad (3.6)$$

Using above equations and superimposed principle, a new concept of pure-fault sequence network for a CIRP integrated system is shown in Fig. 3.4.

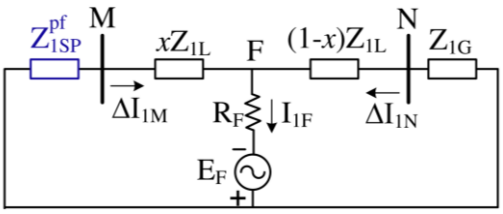

Fig. 3.4: Pure-fault network model of a CIREP

The pure-fault impedance of a solar plant (Z^{pf}_{1SP}) is not same as Z^{pre}_{1SP} and Z^{f}_{1SP}.

The voltage at F during the pre-fault measurement instance is considered as the excitation voltage (E_F) for the pure-fault network. Current distribution property is being applied in Fig. 3.4. The incremental current at bus M (ΔI_{1M}) can be expressed as,

$$\Delta I_{1M} = \frac{(1-x)Z_{1L}+Z_{1G}}{Z^{pf}_{1SP}+Z_{1L}+Z_{1G}} I_{1F} \quad (3.6)$$

Using equations (3.3) and (3.6), Z^{pf}_{1SP} can be expressed as,

$$Z^{pf}_{1SP} = \frac{\left(I^{f}_{1M}+I^{f}_{1N}\right)((1-x)Z_{1L}+Z_{1G})}{I^{f}_{1M}-I^{pre}_{1M}} - (Z_{1L}+Z_{1G}) \quad (3.7)$$

After simplification,

$$Z^{pf}_{1SP} = \frac{\left(I^{pre}_{1M}Z_{MG}-I^{f}_{1M}xZ_{1L}+I^{f}_{1N}Z_{FG}\right)}{I^{f}_{1M}-I^{pre}_{1M}} \quad (3.8)$$

where $Z_{MG} = Z_{1L} + Z_{1G}$ and $Z_{FG} = (1 - x)\, Z_{1L} + Z_{1G}$.

Adding and subtracting E_{1G} of Fig. 3.2, in the numerator of equation (3.8),

$$Z^{pf}_{1SP} = \frac{\left(E_{1G}+I^{pre}_{1M}Z_{MG}\right)-\left(E_{1G}+I^{f}_{1M}xZ_{1L}-I^{f}_{1N}Z_{FG}\right)}{I^{f}_{1M}-I^{pre}_{1M}} \quad (3.9)$$

This can be simplified as

$$V^{pre}_{1M} = E_{1G} + I^{pre}_{1M}Z_{MG}$$

$$V^{f}_{1M} = E_{1G} + I^{f}_{1M}xZ_{1L} - I^{f}_{1N}Z_{FG}$$

Using above-mentioned simplified terms in equation (3.9),

$$Z_{1SP}^{pf} = \frac{V_{1M}^{pre} - V_{1M}^{f}}{I_{1M}^{f} - I_{1M}^{pre}} \quad (3.10)$$

Three phase fault:

For a three-phase fault, apparent impedance calculated by the relay is, $Z_{app}=V_{AM}/I_{AM}$. For a three-phase fault, I_{rM} can be written as $I_{rM} = I_{AM} = I_{1M}$.

From equation (3.6),

$$I_{1F} = \frac{Z_{1SP}^{pf} + Z_{1L} + Z_{1G}}{(1-x)Z_{1L} + Z_{1G}} \Delta I_{1M} \quad (3.11)$$

Due to the homogeneity in a conventional transmission network, the grid equivalent impedance (Z_G) can be expressed in terms of protected line impedance (Z_L) multiplied with a real-valued constant (K) for each sequence component. In this way the equation follows,

$Z_G = K\, Z_L$.

Grid strength is sufficiently large as compared to a solar plant. Therefore, Z_{1G} is smaller than Z_{1L} and Z^{pf}_{1SP}. Neglecting Z_{1G} in the numerator, equation no 3.11 gives,

$$I_{1F} = \Delta I_{1M}\left(\frac{Z_{1SP}^{pf} + Z_{1L}}{Z_{1L}}\right)$$

From Fig. 3.2, α being a gradient of ΔZ, can be expressed as,

$$\alpha_{ABC} = arg\left(\frac{I_F}{I_{rM}}\right) = arg\left(\frac{\left(1+\frac{Z_{1SP}^{pf}}{Z_{1L}}\right)\Delta I_{1M}}{I_{1M}^{f}}\right) \quad (3.12)$$

3.3 Summary:

Apparent impedance gets modulated, so the relay fails to identify the fault. Therefore, an adaptive scheme has been described in this chapter. The algorithm uses the local data from the CIREP side, calculates the actual impedance from the relay point to the fault point, and ensures the correct operation of the distance relay. Distance relays are loaded with the equations derived in this chapter.

CHAPTER 4

Results & Discussion

4.1 System Description

PSCAD version 5 is used for all the simulation study purpose. In this report a simple 2-bus and an IEEE-9 bus system has been studied. Fig 4.1 shows the synchronous generator model used for simulation purpose. It is a 120MVA hydro alternator. Giving a positive value into the **ω** input, the speed of the machine can be controlled directly. A mechanical torque can also be applied at the T_m input to do so. Inertia Constant shows the stored energy in the rotor running at rated speed per machine rating. Typically, Inertia Constant ranges between 2.0 and 6.0 [MWs/MVA].

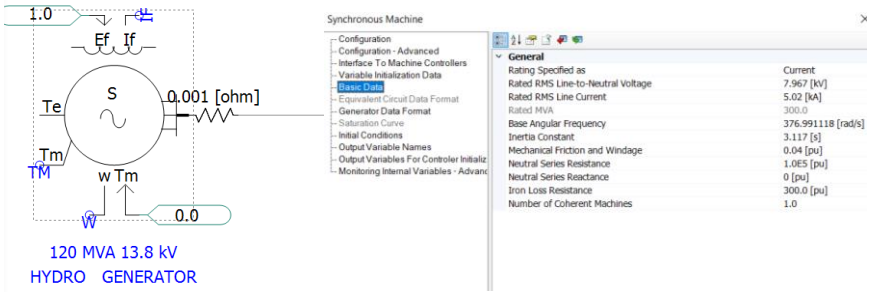

Fig: 4.1 Sync. Gen. model in PSCAD

Coupled capacitor voltage transformer and current transformer is used to make the measured voltage suitable for relaying operation (Fig 4.2).

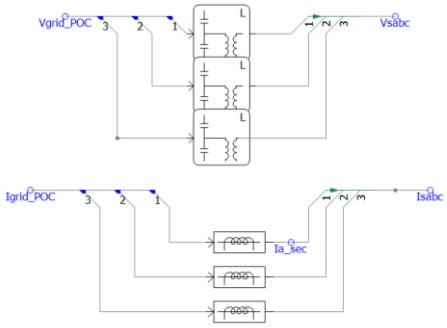

Fig: 4.2 CCVT and CT in PSCAD

The voltage and current obtained from the CCVT and CT are fed into FFT block set (Fig 4.3). Here, the magnitude and phase of each parameter is extracted, and the data are used to calculate the resistance each instant. In chapter 2, the apparent fault impedance calculation is shown. The same is done here also, by using certain impedance calculation block (Fig 4.4). To calculate this apparent impedance magnitude and phase angle of certain phase is required. This data comes from the dedicated FFT block set. After determining the apparent impedance, the R and X values are fed into relays (Fig 4.5). The relays then take necessary action according to the settings given.

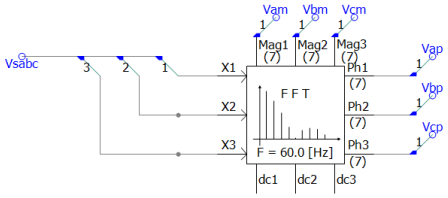

Fig: 4.3 FFT block in PSCAD

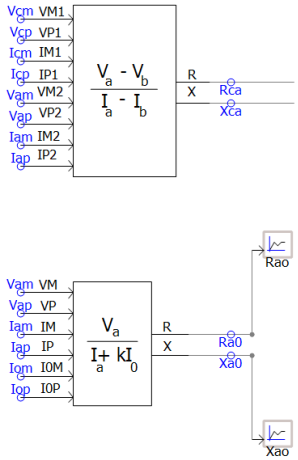

Fig: 4.4 L-L & L-G impedance calculator block in PSCAD

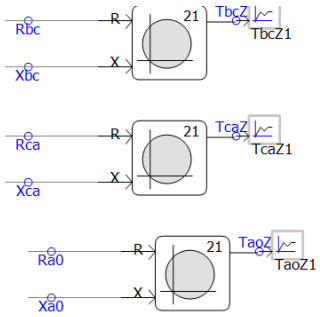

Fig: 4.5 MHO Relays in PSCAD

4.2 Distance protection in two Bus system

A 2-bus system is used to discuss the MHO relay operation. A long transmission line is connecting two buses, consisting of a synchronous generator and a load respectively. A three-phase fault has been introduced at the middle of the line. A circuit breaker is present at the source end bus. This circuit breaker is being operated by an array of mho relays. The Voltage and the current are measured at the source end, then it is fed through CTs and PTs to convert into suitable current and voltage for relay operation.

FFT block extracts the fundamental component of voltage and current for each phase. The magnitude and angle of the fundamental voltage and current is fed into impedance calculation block. The calculated impedance out of the box is fed into mho relay block. A suitable radius is set for the relay to operate. If the impedance is outside of the mho circle, then relay restrain otherwise it trips. In the given model, fault is happening at 10^{th} second.

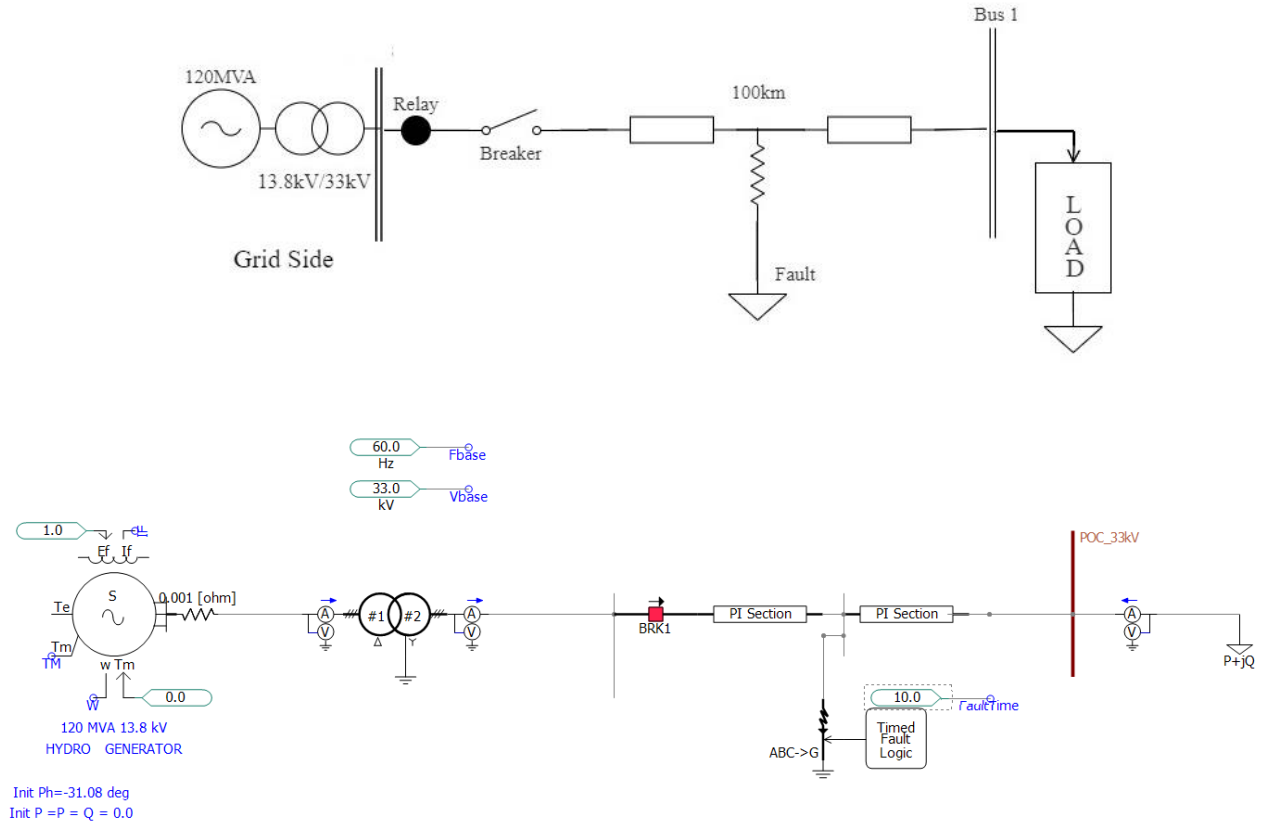

Fig: 4.6 One-line diagram for a conventional two bus system & its PSCAD circuit

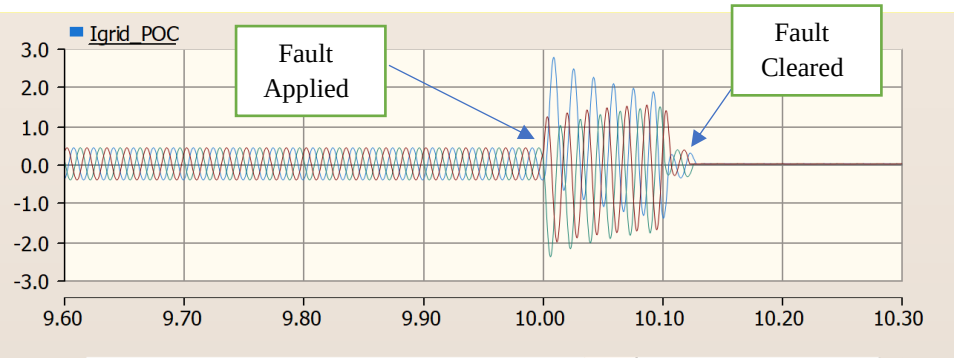

Fig: 4.7 Current response (with fault at 10 sec)

Before 10 sec the current waveform was in stable condition. At 10th second it starts rising. Normally it was 0.35 kA but during fault the magnitude hits 2.3 kA. about 6.5 times rise is observed.

After 2 cycles, the circuit breaker operates and isolates the circuit, the current becomes zero afterwards.

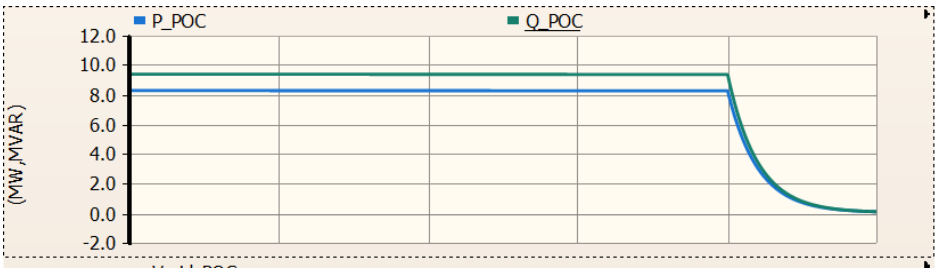

Fig: 4.8 Active and reactive power response

In Fig: 4.8 active and reactive power response before and after the fault is shown. A circuit breaker is used in the system. Due to the breaker operation the power values touches zero in the given Fig 4.8.

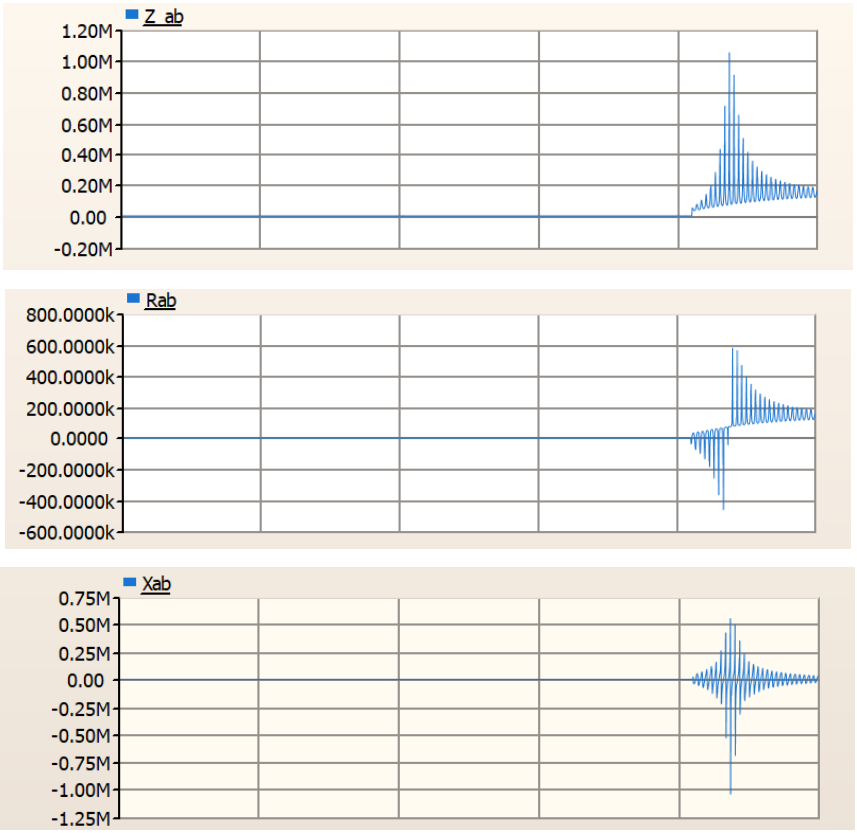

Fig: 4.9 Impedance, resistance, reactance of the system

Fig 4.9 shows the +ve sequence impedance during the fault (between phases A and B). Mho relay uses this impedance value, compares with the set threshold value of impedance and takes protection decision. Mho circle plot (Fig 4.10) validates the aforementioned point.

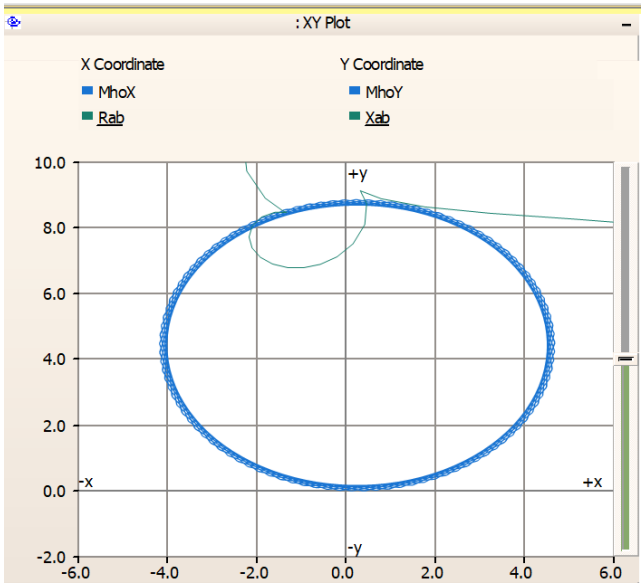

Fig: 4.10 Mho circle and impedance response (R-X plot)

The mho circle for the system shown above is presented in Fig 4.10. The thin line in R-X plot shows the impedance change during a fault. Generally, the impedance at healthy condition of the system remains at the right side of the plot somewhere in 1st or 4th quadrant, based on the system condition. Fault occurring at 10th second makes the thin line (impedance line) to travel inside the mho circle. For power swing or some small oscillation, the impedance curve should not come inside the circle.

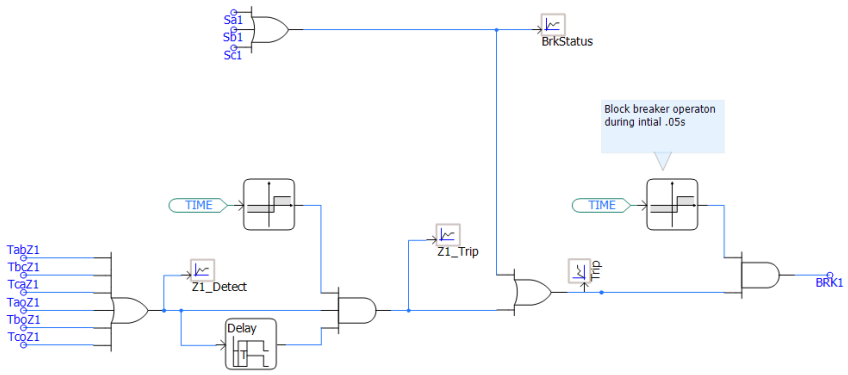

Fig: 4.11 Breaker logic

Fig: 4.11 shows the circuit breaker logic used. TabZ1, TbcZ1, …, Tc0Z1 are the signals coming out of mho relays. These are the digital binary signals (0 stands for no fault detection). All those signals are ORed and the resultant signal is fed into a 3 input AND gate along with two other signals. One is to introduce very small delay in between fault detection and circuit breaker operation, as a result the actual circuit breaker operation timing can be obtained, the other signal is to restrain the circuit breaker to operate at the time of initial transient. Because of the limitation of simulation some transient appears at the beginning of the simulation. This ANDed signal becomes the trip signal for circuit breaker.

4.3 Distance protection in two Bus system with Solar power Plant

Fig 4.12 shows a system with solar PV plant as a source, to study the behaviour of distance protection with renewable energy source. The solar plant is connected with the grid in addition of an inverter in-between. Fig: 4.13 shows the current and voltage response of an CIREP.

Fault at 2 second causes the current waveform to rise. At healthy condition the current magnitude was 0.45 kA and during fault the magnitude raises to 0.65 kA, therefore only 1.48 times of current raise is seen. The value is seen to be reduced drastically, while it was about 6.5 times raise in case of synchronous generator. Inverter current limiting topology causes reduction in current raise during fault.

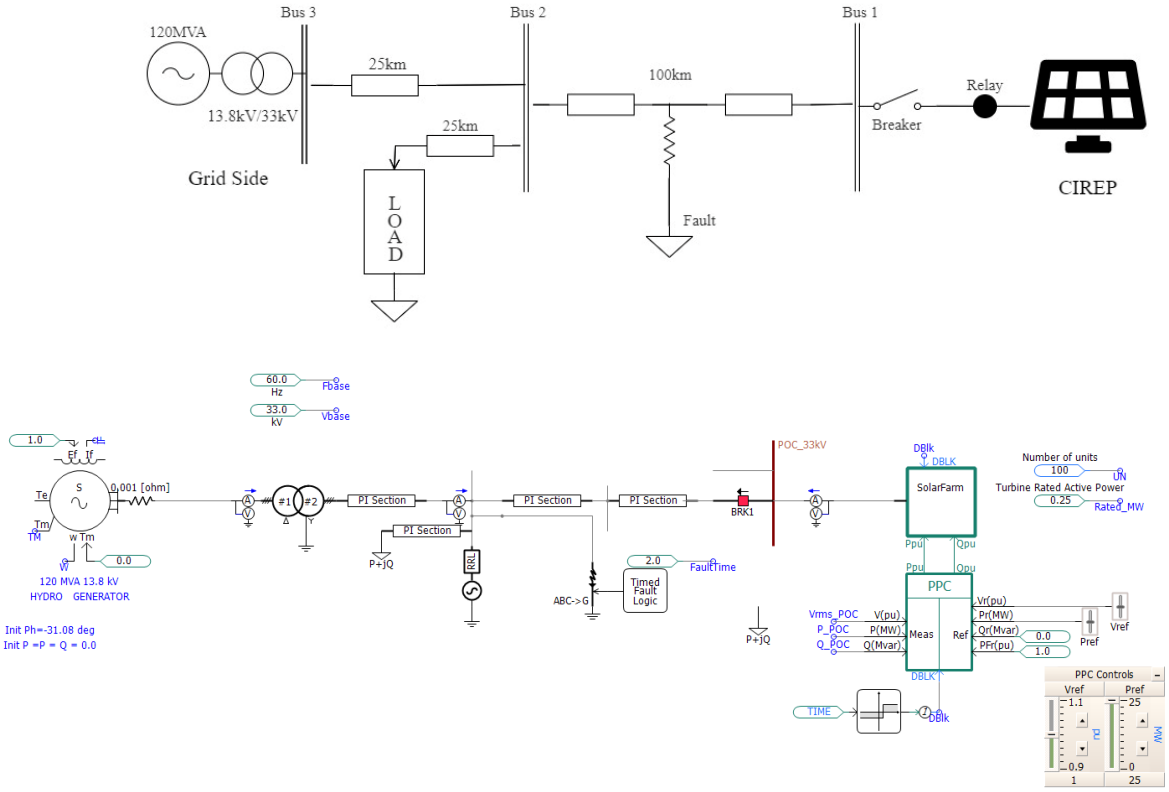

Fig: 4.12 Single line diagram with CIREP for fault analysis & its PSCAD model

Impedance at the PV side bus is given by,

$$Z_W = Z_{WK} + (1 + \frac{I_n}{I_m})R_g \qquad (3.1)$$

R_F is the fault impedance i.e., 0.01 Ω is taken in simulation. While compared to a conventional power system with synchronous generator-based sources, the factor $(1 + \frac{I_n}{I_m})R_g$ is much higher because of the CIREP interface converters' fault current limitation. This introduces nonhomogeneity into the

system unlike a synchronous generator-based network. Which causes a significant phase angle difference between I_n and I_m.

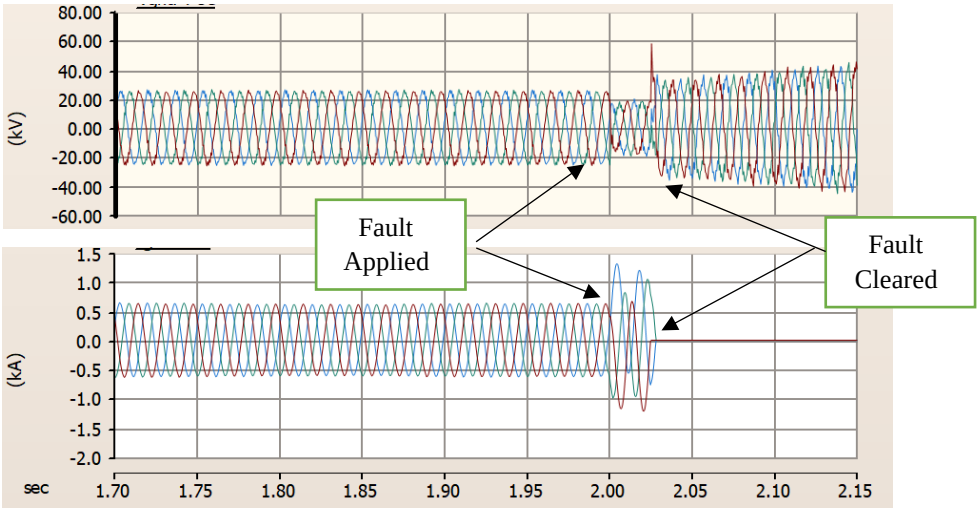

Fig: 4.13 Voltage and current response

Voltage waveform is also affected can be seen from Fig: 4.13.

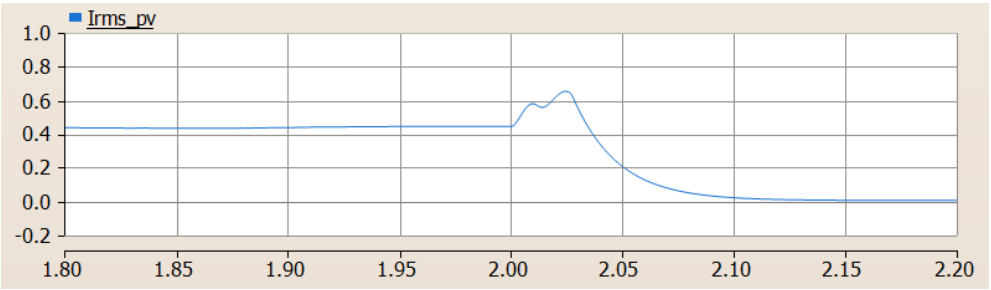

Fig: 4.14 RMS current response from PV side

In Fig 4.14, the impedance seen by the relay is displayed. The impedance immediately before the instant of fault, it is 6.06 Ω. The resistance is 6.06 Ω and the reactance is -0.15 Ω. At this instant the impedance point is outside of the mho relay circle (Fig: 4.15), therefore the relay restrains.

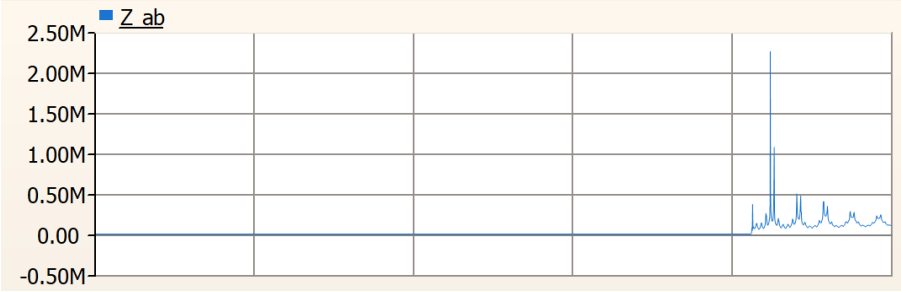

Fig: 4.15 Impedance with CIREP

At the instant of 2.05th sec the reactance is 1.97 Ω and the resistance 3.2 Ω. The point at these instant stays inside the mho circle (Fig 4.16). Therefore, a trip at that instant is observed.

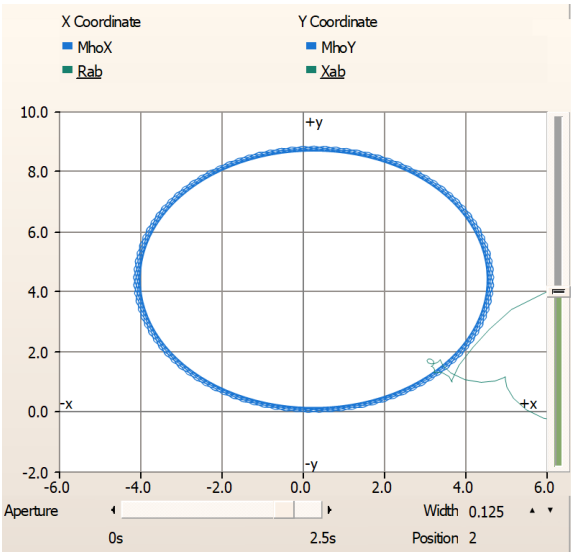

Fig: 4.16 Mho circle and impedance response (R-X plot) with CIREP

Up to now, the system with fault resistance of 0.001 Ω has been studied. Actual system comprises of significant amount of fault resistance.

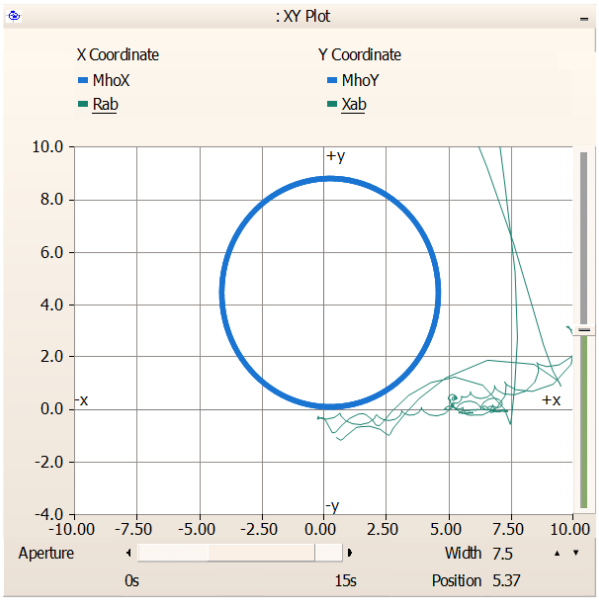

Fig 4.17 Mho circle and impedance response (R-X plot) with CIREP

The R-X plot in Fig 4.17 represents the response of a system with fault resistance of 10 Ω. The impedance remains outside of the mho circle. Therefore, the mho relay could not identify the fault present in the system. As a result, the operation of relay as well as the circuit breaker cannot be seen. The voltage and current waveforms during the fault are shown in Fig 4.18.

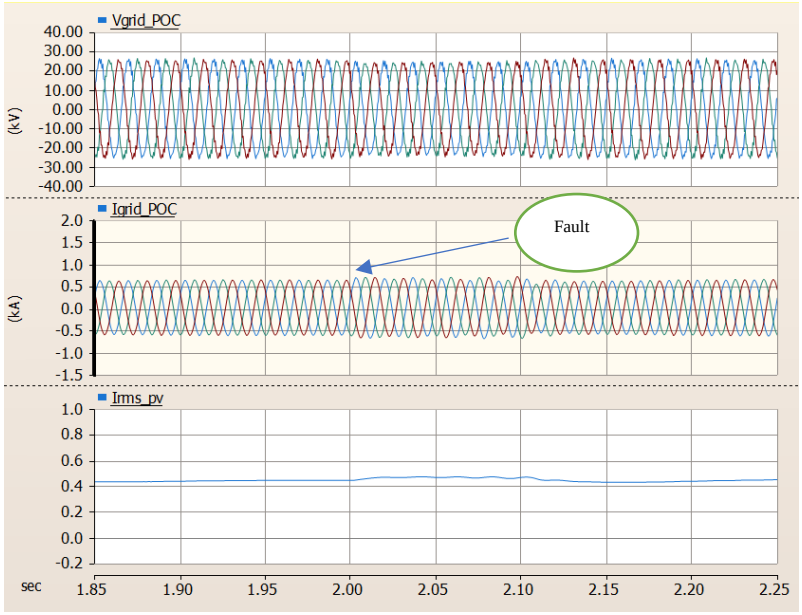

Fig: 4.18 Voltage and current response

Above situations are observed in a power system, when CIREPs are incorporated with a conventional grid. Therefore, the distance relay function/operational strategy needs to be rectified.

4.4 Distance protection in two bus system with quadrilateral relay

To implement the distance protection based on quadrilateral relay characteristics, the line parameters are first analysed. The positive sequence impedance of the line is 0.00258 + j0.051 Ω/km. 120 km long transmission line is being protected here. If the zone 1 is considered as 90% of the total line, the protected portion becomes 0.9×120=108 km.

Therefore, the total line impedance of the protected line becomes (0.279+j5.463) Ω. From this specification the magnitude of the impedance becomes 5.47 Ω. To set the quadrilateral relay 5.5 Ω is taken as the value (Fig 4.19).

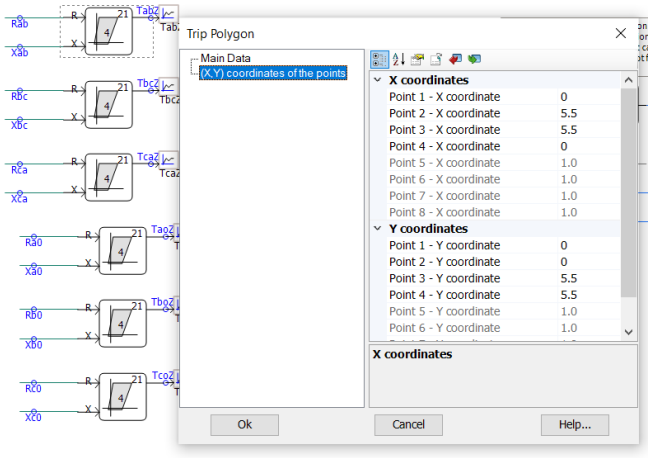

Fig: 4.19 Quadrilateral relay settings

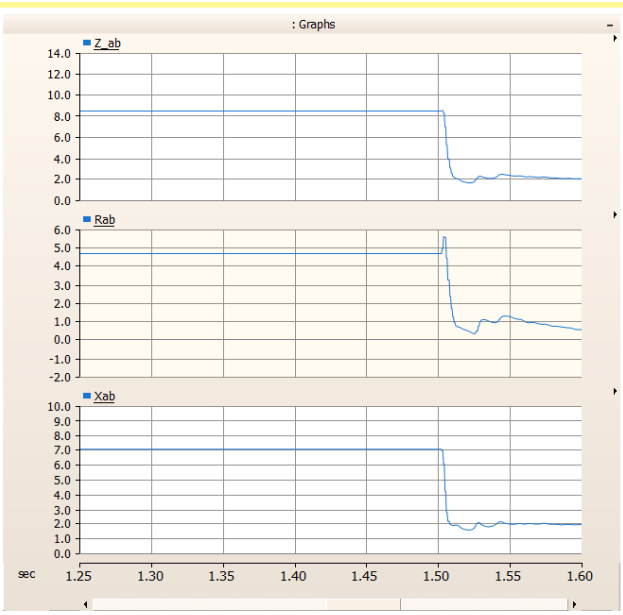

Fig: 4.20 Impedance response before and after fault

In Fig 4.20, how the value of the impedance changes is portrayed. The fault is happening in the system at 1.5 s. At this moment the impedance value decreases. The magnitude of Z is approximately 2 Ω, comes under the jurisdiction of the quadrilateral relay employed in the system. This result can be verified very easily with the R-X plane plotting (Fig 4.21).

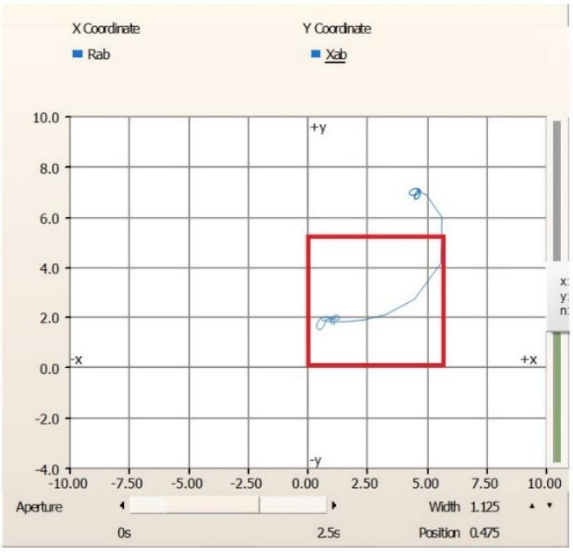

Fig: 4.21 Quadrilateral relay operation in RX plane

For simplicity purpose, square type relay characteristics is been deployed. It can be observed that the impedance point lies outside of the square before the fault but when the fault happens the points comes inside the square, as a result the relay trips.

4.5 Mho based distance protection in IEEE-9 bus system with solar plant

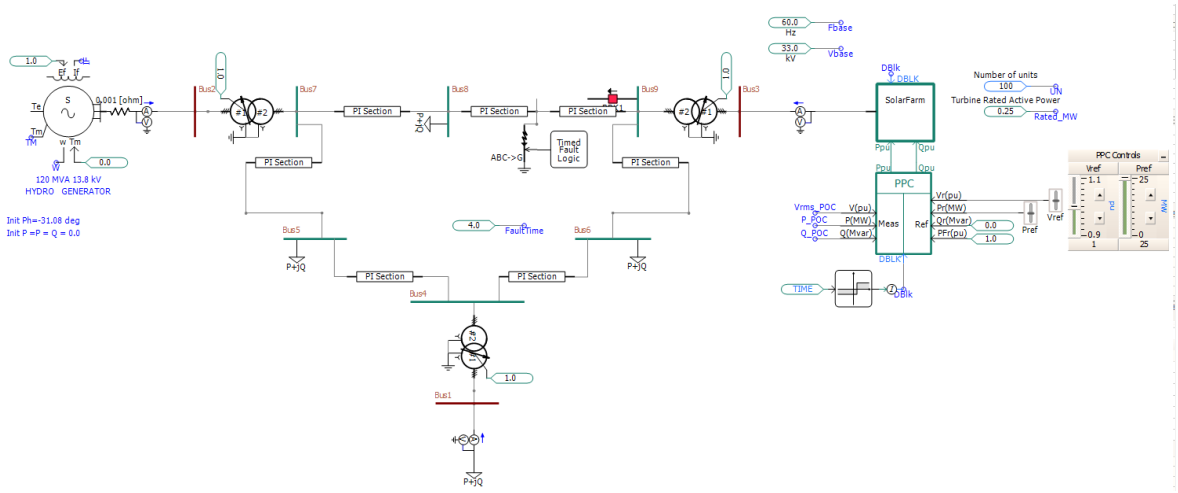

Fig: 4.22 IEEE-9 Bus system with CIREP

To understand the operation of the distance protection scheme in broad aspect, the IEEE-9 bus system (Fig 4.22) has been studied. A single circuit breaker and relaying scheme is employed at the CIREP side. The protection decision is made based on the voltage and current profile a the CIREP side. Fault is happening at 4th second. During the fault, the circuit breaker isolates line 8-9 from the CIREP side. The voltage and current response at the solar plant side is shown in Fig 4.23. A momentary dip of voltage and increment of current profile is observed.

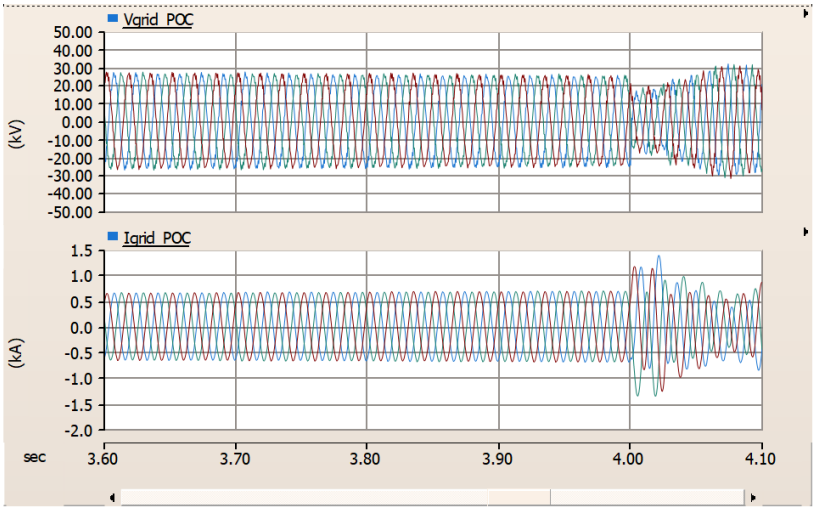

Fig: 4.23 Voltage and current response before and after fault

4.6 Adaptive Scheme in PSCAD

Logic used:

Objective is to find α and hence Z_{MF}. Equation (3.12) gives the value of α for a three-phase fault. Voltage and current coming out of the CIREP is processed and magnitude, phase fundamental component is extracted. These values give Z_{1SP}^{pf} from equation no (3.10). The line impedance Z_{1L} is already available. Equation (3.5) gives ΔI_{1M}. All these parameters are separately obtained using PSCAD logic blocks and α is determined.

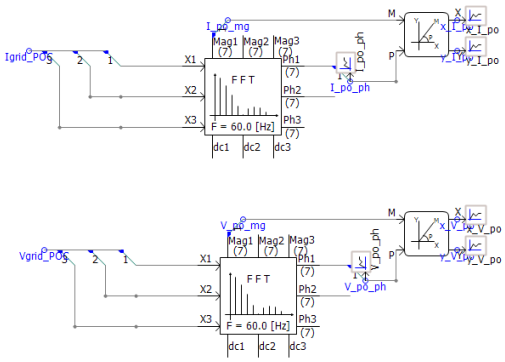

Fig: 4.24 Magnitude, phase of voltage & current extraction

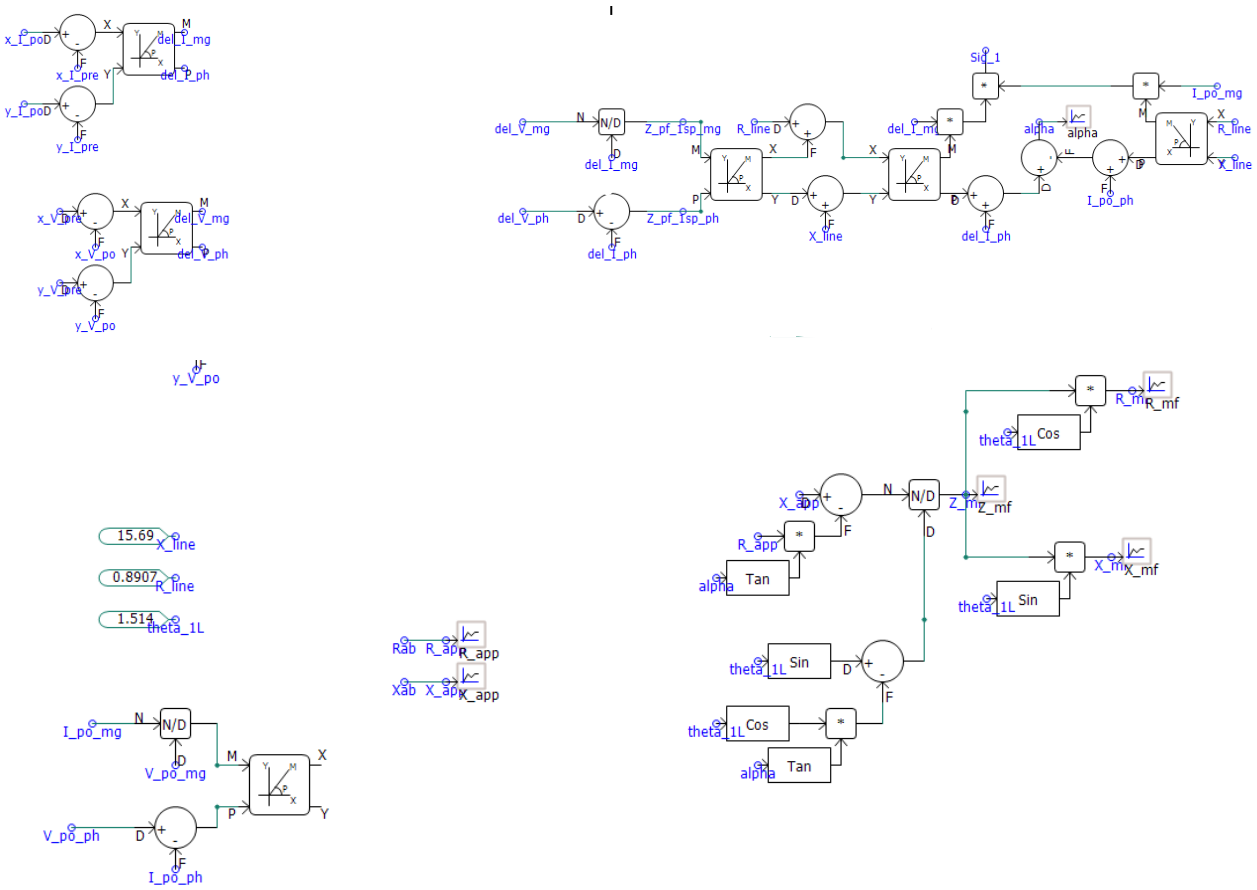

Fig: 4.25 PSCAD logics for adaptive relaying

After successful determination of α, equation (3.2) is used to determine the Z_{MF}. This parameter is fed into MHO relay.

4.7 Performance analysis of the Adaptive Scheme

Fig. 4.26 indicates the apparent impedance seen by the relay when R_F =0.001 Ω. It is to be noted that after the fault at 2 s, the impedance drops at 0.51 Ω. As the fault impedance is negligible the Z_{app} obtained at this situation can be taken as the impedance of the line up to the fault point.

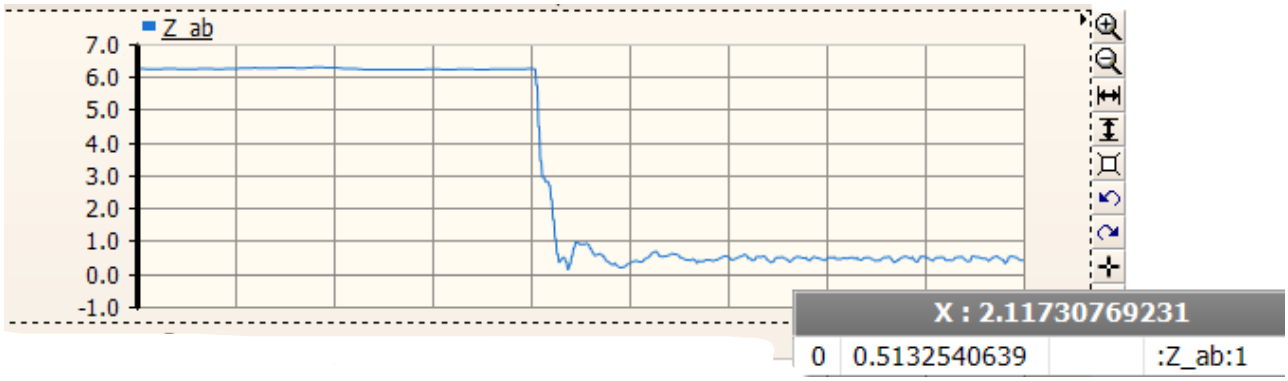

Fig: 4.26 Apparent impedance with R_F =0.001Ω

Fig. 4.27 shows the response of the system when the fault resistance is taken as 10 Ω. At this scenario, after occurrence of fault Z_{app} becomes 3.57 Ω. So, previously mentioned parameter ΔZ is coming in account.

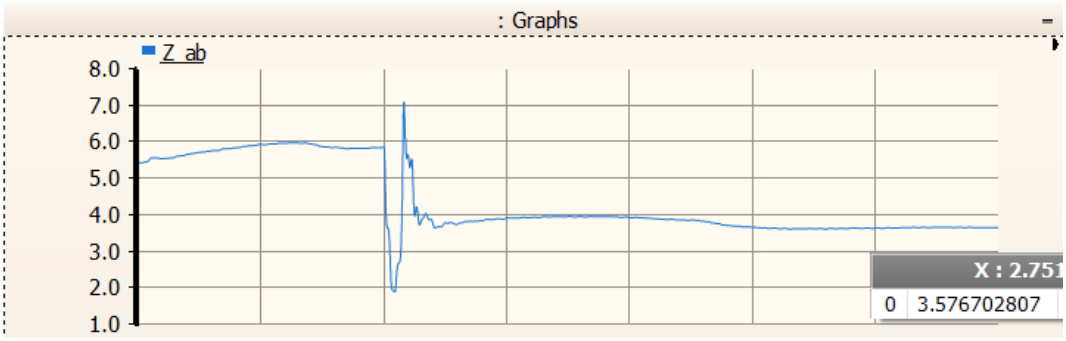

Fig: 4.27 Apparent impedance with R_F=10 Ω

Adaptive method calculates the impedance up to the fault point. Fig. 4.28 shows the impedance (Z_{MF}) calculated using adaptive method is 0.51 when R_F is 0.001 Ω. That exactly matches the impedance up to the fault point obtained in previous case.

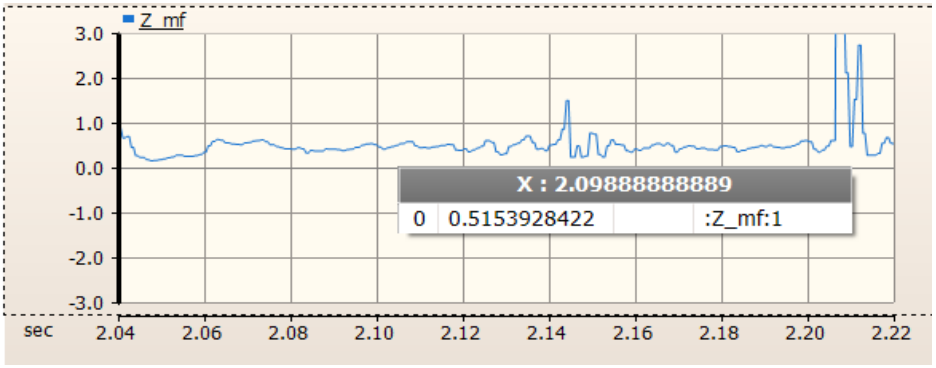

Fig: 4.28 Impedance obtained from adaptive scheme (R_F=0.001 Ω)

Fig. 4.29 depicts the impedance calculated by the adaptive algorithm when R_F=10 Ω. Z_{MF} is nearly 0.62 Ω. To be noted, without adaptive algorithm that impedance seen by the relay was 3.57 Ω. That value was supposed to be near to 0.51 Ω. Using adaptive algorithm, difference has been eliminated hugely.

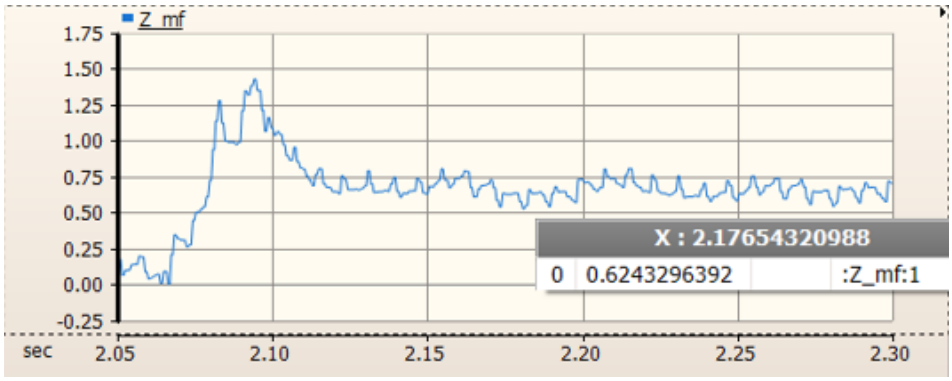

Fig: 4.29 Impedance obtained from adaptive scheme (R_F=10 Ω)

Fig. 4.30 shows the Relay response with the impedance obtained from adaptive algorithm.

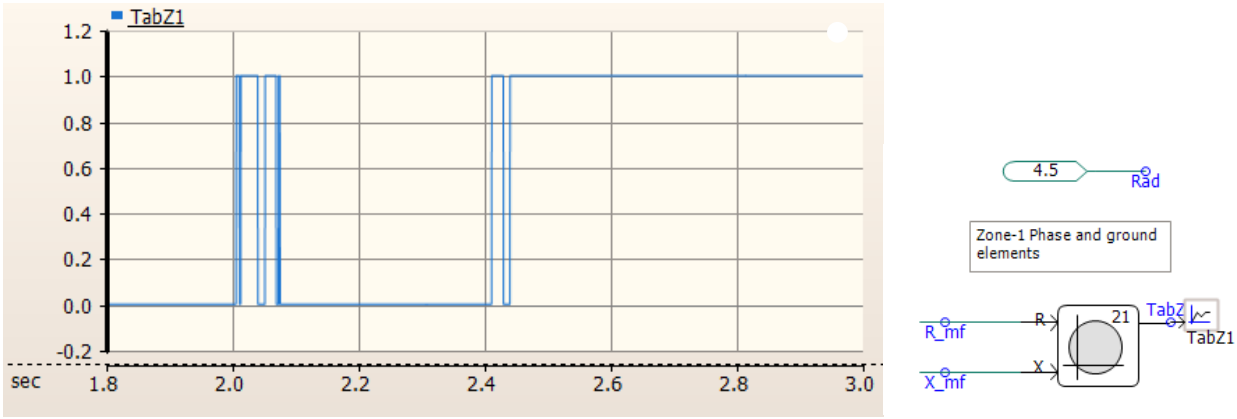

Fig: 4.30 Relay response with the impedance obtained from adaptive algorithm

4.8 Summary

Chapter 4 indicates the conventional relaying operation with synchronous generator. The results are compared with CIREPs added systems. It is observed, when fault resistances are negligible then conventional system works fine. However, introduction of fault resistance blocks the relay operation. Later in the chapter, the adaptive scheme results are portrayed. It is seen, how the adaptive scheme efficiently identifies the fault impedance, irrespective of the presence of fault resistance.

CHAPTER 5
Hardware In Loop Implementation

5.1 Real-time Simulation

A computerized model of a physical system that can operate at the same rate of real-world time is referred to as a "real-time simulation." The computer model, therefore, operates at the same speed as the actual physical system. Time advances in equal-sized steps during discrete-time simulation. Various problem-solving methods employ variable time steps. These methods are used to solve nonlinear systems and high-frequency dynamics; however, they are inappropriate for real-time simulation. Each variable or system state is solved successively as a function of variables and states after the preceding time step to solve mathematical functions and equations at a particular time step. The amount of real-time required during a discrete-time simulation to compute all equations and functions of a system during a given time step may be shorter or longer than the simulation timestep. The moment at which a result comes is unimportant in both situations. The goal of the offline simulation is typically to get findings as quickly as possible. The complexity of the mathematical model used by the system affects how quickly it solves problems. The real-time simulation must, in other words, generate the internal variables and output in the same amount of time as its physical counterpart.

5.2 speedgoat[23]

The real-time target machines like Speedgoat is ideal for small-scale real-time controller or plant simulator with perfect MATLAB & Simulink workflow integration. Rapid design, test, run, and deploying high-performance controls applications and running smaller-scale plant simulations are possible in Speedgoat. MATLAB & Simulink workflow can be integrated with the “Speedgoat” through Simulink real time.

5.3 MATLAB model description

A two-bus system showed in Fig. 5.1 has been used for the above-mentioned purpose. A 250 kW capacity solar power plant is present at bus-1 and bus-2 is connected with a 3phase source that replicates a grid. Transmission lines are operating at 25 kV. A 30 MW 2 MVar load is present at grid side. A fault has been introduced at the middle of the transmission line. Voltage and current

rating at bus-1 and bus-2 are used for protection operation. Signal Trip_B1 operates the breaker at renewable side and Trip_B2 takes care of the breaker at grid side (Fig 5.2). Protection logic implemented for this purpose is depicted in Fig. 5.3.

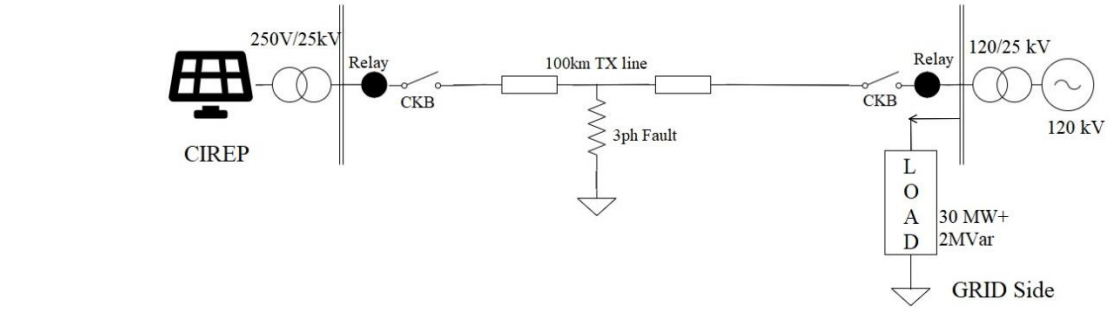

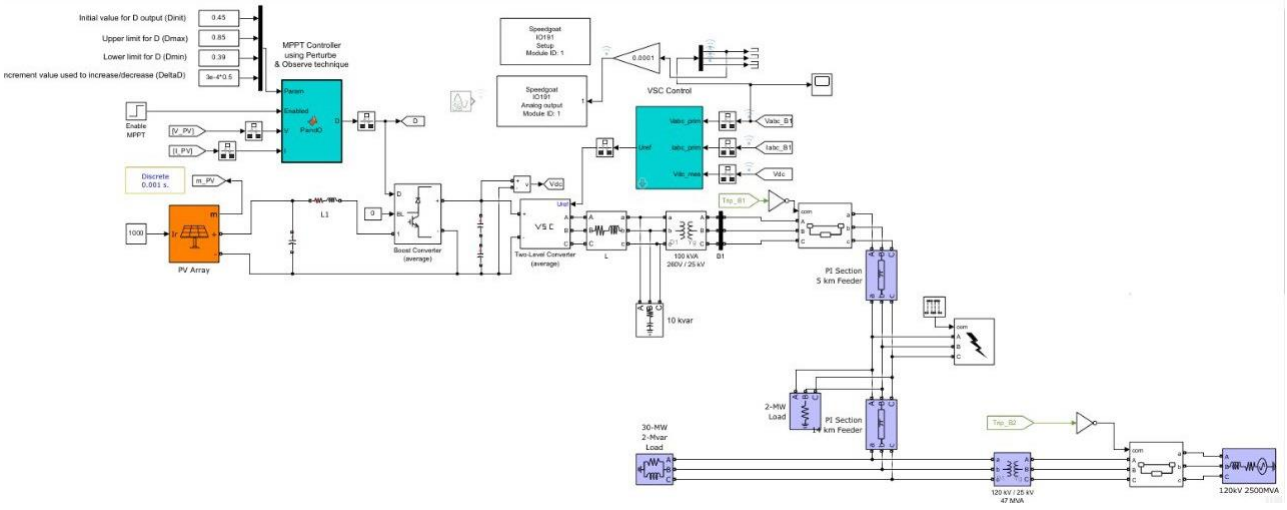

Fig: 5.1 Circuit modelled in Simulink for Speedgoat implementation

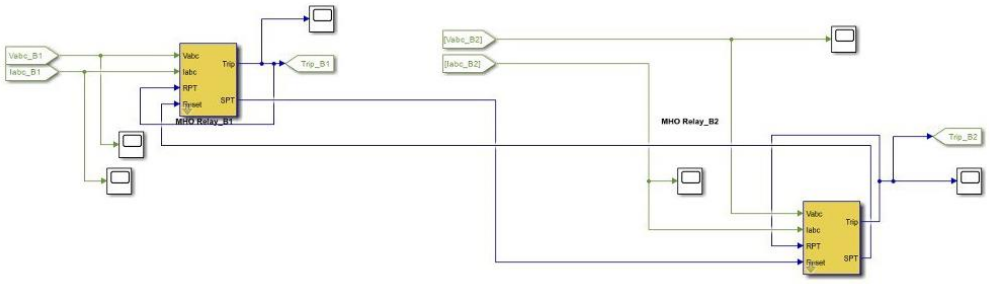

Fig: 5.2 Relays modelled in Simulink for Speedgoat implementation

Measurement unit block shown in Fig. 5.3, it takes 3 phase voltage and current as input and converts the data into fundamental components. Fundamental voltage and currents out of the Measurement unit block, are used to calculate impedances. Equation no 2.5 and 2.10 are used for the calculation purpose. Fault detection logics are present at fault detection block. Based on the value of transmission line parameters and its length, the fault detection quantities are set. The last block is the trip block, that feds trip signals in case of a fault present in the system.

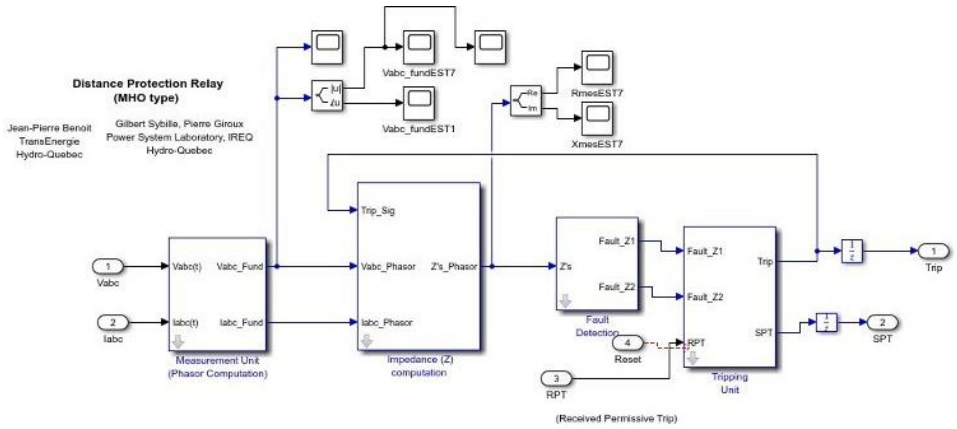

Fig: 5.3 Logic inside distance relay

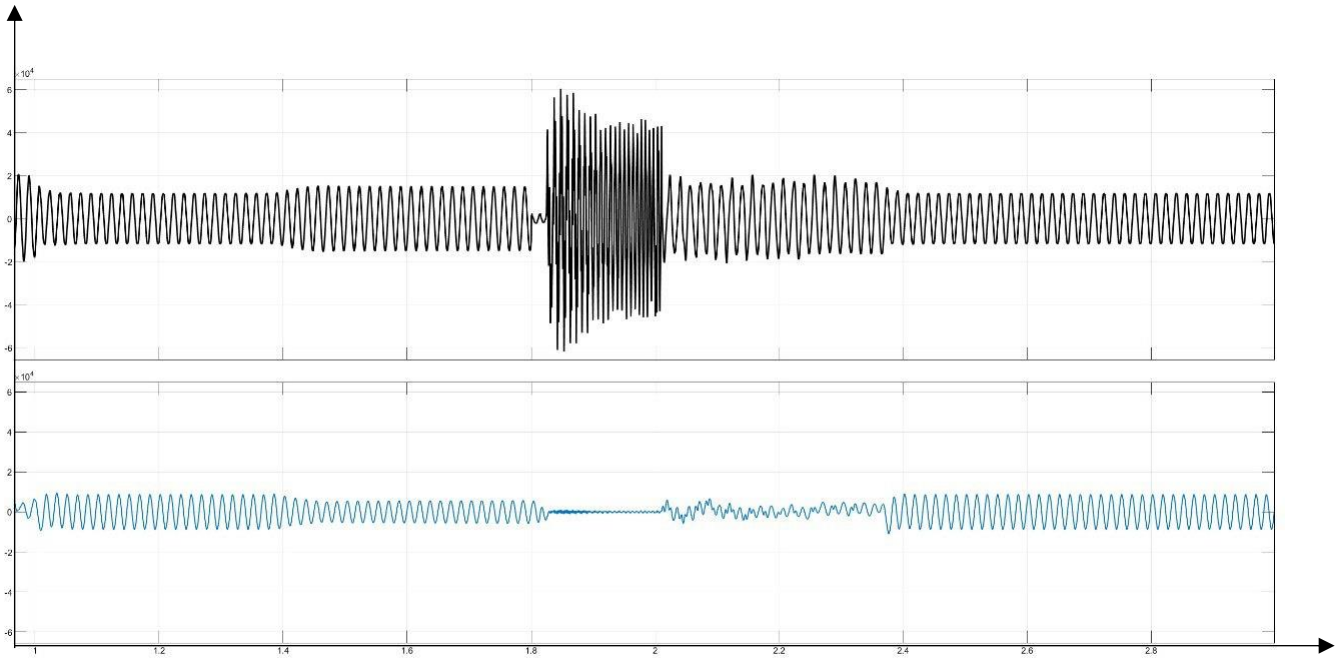

Fig: 5.4 Current & Voltage response recorded in Simulink

Fig. 5.4 shows voltage and current wave for before and after fault at renewable side. Current becomes zero as the breaker is open. Trip signal associated with the renewable side breaker is shown in Fig. 5.5.

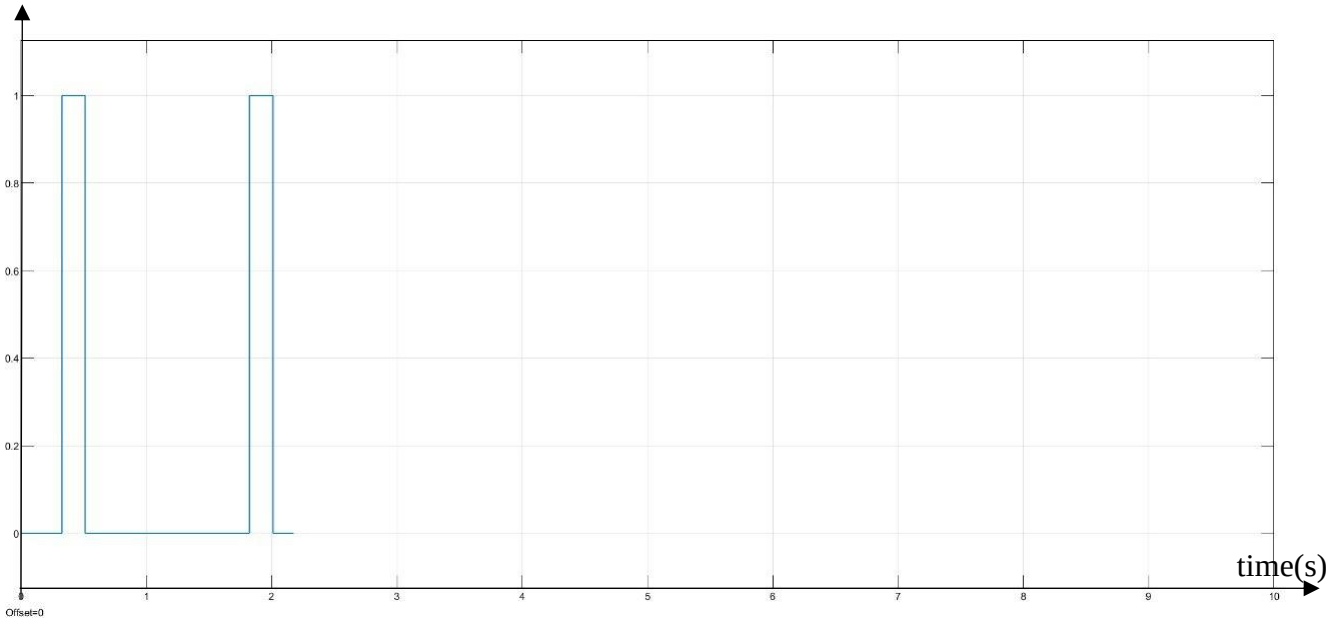

Fig: 5.5 Relay Trip signal

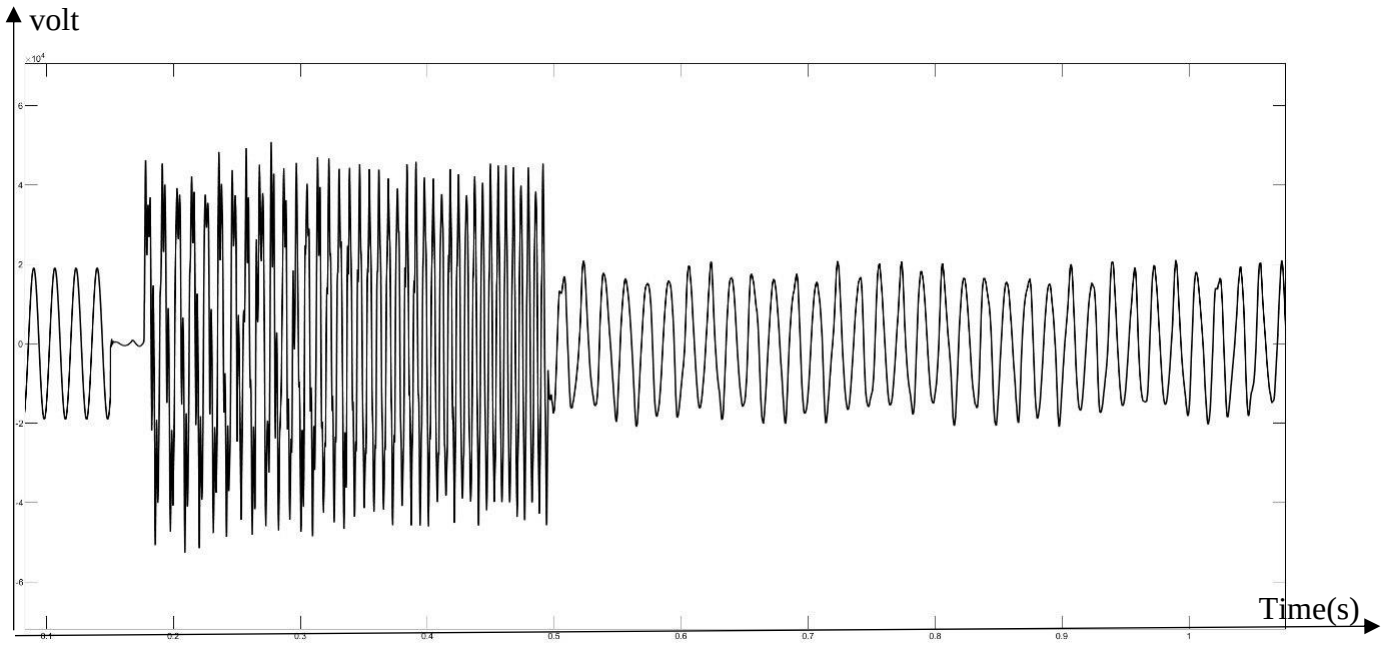

Fig: 5.6 Zoomed Voltage response during fault

Fig 5.6 shows the voltage response at renewable side. This MATLAB model is uploaded in Speedgoat real time simulation system. The step time is taken as 0.001 sec. The voltage response recorded in DSO is shown in Fig. 5.7.

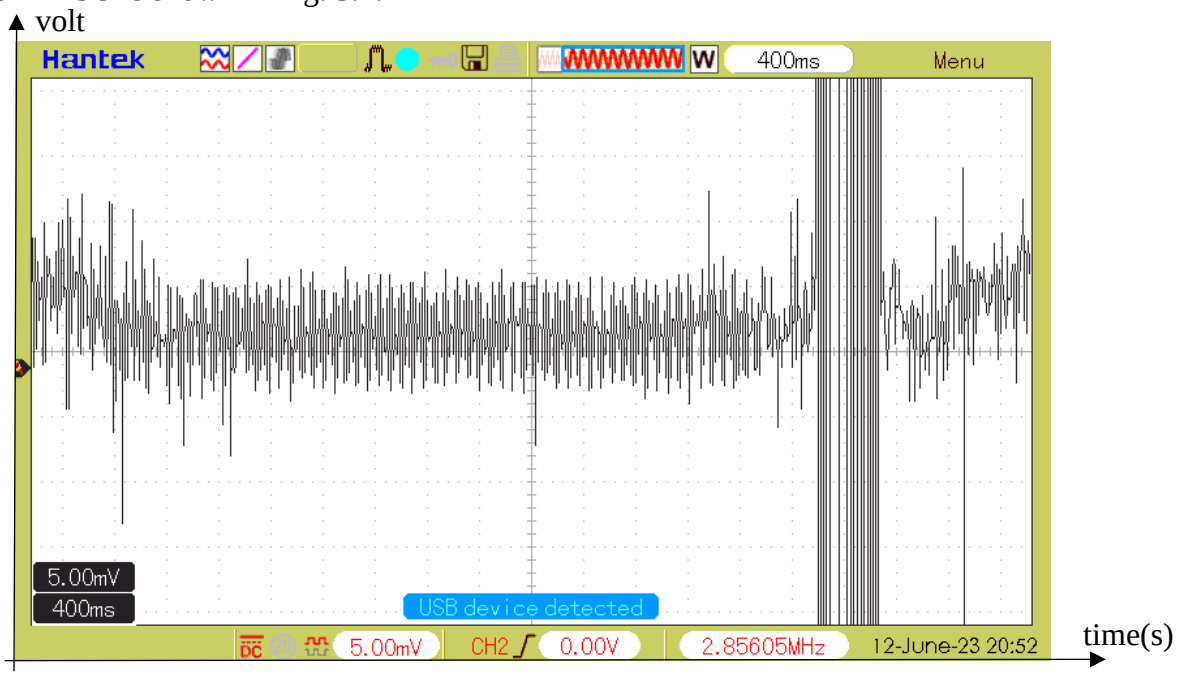

Fig: 5.7 Voltage response during fault from DSO

5.4 Summary

The results shown in Chapter 4 have been verified using the Speedgoat hardware set. Real-time simulation portrays the actual scenario that cannot be observed through ordinary simulation software. It also ensures the reliability of the operation of the adaptive scheme.

CHAPTER 6
Conclusion & Future Scope

6.1 Conclusion:

CIREPs creates disturbance in distance protection scheme due to different control strategies associated with the inverter present that connect the renewable energy plant with the grid. The side-by-side comparison is conducted for conventional synchronous generator and CIREPs by introducing a fault in the system to study the behaviour in distance protection. The fault current limitation in CIREPs, is elaborately discussed in this report and also discussed how it may create trouble in case of distance protection. Drastically reduction of fault current shows an alarming situation and as a consequence distance protection may fail. Quadrilateral relay might be deployed to counter the situation arises due to the CIREP with fault impedance. But it may not differentiate the highly loaded condition or the power swing. Therefore, to deal with the situation adaptive distance protection could be the only solution.

6.2 Scope for Future Work

1. Adaptive Distance scheme with quadrilateral relay

   In a system with CIREP the conventional protection scheme fails. Therefore, some additional protection algorithm is needed to be implemented. Here comes adaptive distance protection algorithm. The quadrilateral relay operation area can be customized according to the system demand. This report portrayed adaptive distance protection with MHO relay. In such scenario some chattering is seen in relay signal. That can possibly be omitted with quadrilateral relay.
2. Power swing in system

   Due to the power swing, large variation may be seen in voltage, current and power flow. And hence maloperation in distance relaying is seen. The operation of the distance relay must be

blocked during such condition. Power swing blocking (PSB) function need to be deployed in distance relays. Deploying the aforementioned adaptive scheme, it can also be mitigated.

3. Check the reliability with higher bus system in Speedgoat. This report has shown the response in an IEEE 9 bus system in PS CAD. Higher IEEE bus system (like 39 Bus) might be employed in Speedgoat real time simulator to validate the response.
4. Hardware in-loop can be checked. Microprocessors (like, TI Launchpad works with Simulink system) need to be loaded with distance protection algorithms. The voltage and current data, coming out of the Speedgoat output ports, could be used as input for the microprocessor. The calculated trip signal out of the device returns to the Speedgoat system. Reliability will increase, and the microprocessor will act as a numerical relay.

PUBLICATIONS FROM THE THESIS

Conference Papers

Ujjal Banik, Athul Jose P and Deepak M, "Adaptive mho Relay Based Distance Protection Scheme on CIREP System," 3rd International Conference on Power Electronics, Smart Grid, and Renewable Energy (PESGRE 2023), During 17th-20th Dec 2023, at Hotel Hycinth, Trivandrum, Kerala, India. (Submitted)

REFERENCES

[1] A. Morales, X. Robe, M. Sala, P. Prats, C. Aguerri, and E. Torres, “Advanced grid requirements for the integration of wind farms into the Spanish transmission system,” IET Renew. Power Gen., vol. 2, no. 1, pp. 47–59, Mar. 2008.

[2] A. Hooshyar, M. A. Azzouz, and E. F. El-Saadany, “Distance protection of lines emanating from full-scale converter-interfaced renewable energy power plants—Part I: Problem statement,” IEEE Trans. Power Del., vol. 30, no. 4, pp. 1770–1780, Aug. 2015.

[3] Y. Fang, K. Jia, Z. Yang, Y. Li and T. Bi, "Impact of Inverter-Interfaced Renewable Energy Generators on Distance Protection and an Improved Scheme," in IEEE Transactions on Industrial Electronics, vol. 66, no. 9, pp. 7078-7088, Sept. 2019, doi: 10.1109/TIE.2018.2873521.

[4] Y. Liang, W. Li and W. Zha, "Adaptive Mho Characteristic-Based Distance Protection for Lines Emanating From Photovoltaic Power Plants Under Unbalanced Faults," in IEEE Systems Journal, vol. 15, no. 3, pp. 3506-3516, Sept. 2021, doi: 10.1109/JSYST.2020.3015225.

[5] Z. Yang, K. Jia, Y. Fang, Z. Zhu, B. Yang and T. Bi, "High-Frequency Fault Component-Based Distance Protection for Large Renewable Power Plants," in IEEE Transactions on Power Electronics, vol. 35, no. 10, pp. 10352-10362, Oct. 2020, doi: 10.1109/TPEL.2020.2978266.

[6] S. Paladhi and A. K. Pradhan, "Adaptive Distance Protection for Lines Connecting Converter-Interfaced Renewable Plants," in IEEE Journal of Emerging and Selected Topics in Power Electronics, vol. 9, no. 6, pp. 7088-7098, Dec. 2021, doi: 10.1109/JESTPE.2020.3000276.

[7] M. Zolfaghari, R. M. Chabanlo, M. Abedi and M. Shahidehpour, "A Robust Distance Protection Approach for Bulk AC Power System Considering the Effects of HVDC Interfaced Offshore Wind Units," in IEEE Systems Journal, vol. 12, no. 4, pp. 3786-3795, Dec. 2018, doi: 10.1109/JSYST.2017.2760139.

[8] H. Teimourzadeh, B. Mohammadi-Ivatloo and M. Shahidehpour, "Adaptive Protection of Partially Coupled Transmission Lines," in IEEE Transactions on Power Delivery, vol. 36, no. 1, pp. 429-440, Feb. 2021, doi: 10.1109/TPWRD.2020.2983138.

[9] Power System Protection. Paul M. Anderson, Charles Henville, Rasheek Rifaat, Brian Johnson, Sakis Meliopoulos. First published:31 December 2021. Print ISBN:9781119513148 |Online ISBN:9781119513100 |DOI:10.1002/9781119513100

[10] P. Regulski, W. Rebizant, M. Kereit and S. Schneider, "Adaptive Reach of the 3rd Zone of a Distance Relay With Synchronized Measurements," in IEEE Transactions on Power Delivery, vol. 36, no. 1, pp. 135-144, Feb. 2021, doi: 10.1109/TPWRD.2020.2974587.

[11] "Transmission Line Protection Using Digital Technology", Vijay H. Makwana, Bhavesh R. Bhalja. Springer Nature, 2016

[12] Z. Yang, Q. Zhang, W. Liao, C. L. Bak and Z. Chen, "Harmonic Injection Based Distance Protection for Line With Converter-Interfaced Sources," in IEEE Transactions on Industrial Electronics, vol. 70, no. 2, pp. 1553-1564, Feb. 2023, doi: 10.1109/TIE.2022.3159971.

[13] Yuxi Wang, Minghao Wen, Yu Chen, "A novel directional element for transmission line connecting inverter-interfaced renewable energy power plant", International Journal of Electrical Power & Energy Systems, Volume 145, 2023, 108682, ISSN 0142-0615,

[14] Mohammad Meraj Alam, Helder Leite, Jun Liang, Adriano da Silva Carvalho, "Effects of VSC based HVDC system on distance protection of transmission lines", International Journal of Electrical Power & Energy Systems, Volume 92, 2017, Pages 245-260, ISSN 0142-0615

[15] S. Paladhi and A. K. Pradhan, "Adaptive Fault Type Classification for Transmission Network Connecting Converter-Interfaced Renewable Plants," in IEEE Systems Journal, vol. 15, no. 3, pp. 4025-4036, Sept. 2021, doi: 10.1109/JSYST.2020.3010343.

[16] J. Patel, Ujjaval, Chothani, Nilesh G. and Bhatt, Praghnesh J.. "Distance Relaying with Power Swing Detection based on Voltage and Reactive Power Sensitivity " *International Journal of Emerging Electric Power Systems*, vol. 17, no. 1, 2016, pp. 27-38. https://doi.org/10.1515/ijeeps-2015-0109

[17] E. Buraimoh and I. E. Davidson, "Laboratory Procedure for Real-Time Simulation Experiment of Renewable Energy Systems on OPAL-RT Digital Simulator," 2022 10th International Conference on Smart Grid (icSmartGrid), Istanbul, Turkey, 2022, pp. 221-226, doi: 10.1109/icSmartGrid55722.2022.9848570.

[18] H. Mortazavi, H. Mehrjerdi, M. Saad, S. Lefebvre, D. Asber and L. Lenoir, "A Monitoring Technique for Reversed Power Flow Detection With High PV Penetration Level," in IEEE

Transactions on Smart Grid, vol. 6, no. 5, pp. 2221-2232, Sept. 2015, doi: 10.1109/TSG.2015.2397887.

[19] K. El-Arroudi and G. Joós, "Performance of Interconnection Protection Based on Distance Relaying for Wind Power Distributed Generation," in IEEE Transactions on Power Delivery, vol. 33, no. 2, pp. 620-629, April 2018, doi: 10.1109/TPWRD.2017.2693292.

[20] A. Banaiemoqadam, A. Hooshyar and M. A. Azzouz, "A Control-Based Solution for Distance Protection of Lines Connected to Converter-Interfaced Sources During Asymmetrical Faults," in IEEE Transactions on Power Delivery, vol. 35, no. 3, pp. 1455-1466, June 2020, doi: 10.1109/TPWRD.2019.2946757.

[21] Amir Ghorbani, Hasan Mehrjerdi,"Distance protection with fault resistance compensation for lines connected to PV plant", International Journal of Electrical Power & Energy Systems, Volume 148, 2023, 108976, ISSN 0142-0615,

[22] Y. Liang, W. Li and Y. Huo, "Zone I Distance Relaying Scheme of Lines Connected to MMC-HVDC Stations During Asymmetrical Faults: Problems, Challenges, and Solutions," in IEEE Transactions on Power Delivery, vol. 36, no. 5, pp. 2929-2941, Oct. 2021, doi: 10.1109/TPWRD.2020.3030332.

[23] https://www.speedgoat.com/knowledge-center